The *autophagy-related genes AtATG5* and *AtATG7* influence reserve mobilisation and responses to ABA during seed germination in *Arabidopsis thaliana*

Estefanía Contreras[1], Elena Pastor-Mora[1], Mar Aylón-Rodríguez[1], Mar González-Ceballos[1], Miguel Ángel Delgado-Gutiérrez[1], Inmaculada Sánchez-Vicente[3], Óscar Lorenzo[3], Jesús Vicente-Carbajosa[1,2]*, Raquel Iglesias-Fernández[1,2]*

[1]Centro de Biotecnología y Genómica de Plantas-Severo Ochoa (CBGP, UPM-INIA), Universidad Politécnica de Madrid (UPM) - Instituto Nacional de Investigación y Tecnología Agraria y Alimentaria (CSIC/INIA), 28223 Pozuelo de Alarcón, Spain
[2]Departamento de Biotecnología-Biología Vegetal, Escuela Técnica Superior de Ingeniería Agronómica, Alimentaria y de Biosistemas, UPM, 28040 Madrid, Spain
[3]Departamento de Botánica y Fisiología Vegetal, Instituto de Investigación en Agrobiotecnología (CIALE), Facultad de Biología, Universidad de Salamanca, C/ Río Duero 12, 37185 Salamanca, Spain.

*For correspondence: (email: raquel.iglesias@upm.es and jesus.vicente@upm.es)

ABSTRACT

Autophagy is a cell recycling mechanism that degrades cytoplasmic components. Although classically considered a non-selective bulk degradation mechanism, autophagy also functions selectively. Here, we investigate the impact of autophagy on seed development by studying the autophagy-related (ATG) genes *AtATG5* and *AtATG7* in Arabidopsis, focusing on their role in ABA responses. Seeds of *atg5* and *atg7* mutants germinate significantly slower than Col-0, especially in the presence of ABA. Transcriptomic analyses comparing imbibed *atg7* and Col-0 seeds reveal differences in gene expression associated with lipid storage and seed maturation ontology categories. Germinating seeds of *atg* mutants show histochemical alterations in the organisation of lipid droplets and protein storage vacuoles (PSV) in the emerging radicle. Notably, immunolocalization of ATG8 is observed in PSV in Col-0, but not in *atg* mutants. In the presence of ABA, approximately 10% of the transcriptome induced in *atg7* and repressed in Col-0 has been reported to be under control of the transcription factors ABI3 and ABI5, master regulators of ABA signaling in the seed. Yeast-two hybrid assays confirmed their direct interaction with the autophagy machinery through ATG8. Interestingly, the decrease in ABI5 observed in Col-0 seeds after imbibition is delayed in *atg* mutants, which also show altered accumulation in developing seeds of the ABI5 homolog bZIP67 that regulates reserve biosynthesis. Taken together, our data highlight the relevance of autophagy in controlling seed reserve mobilisation, its impact on seed germination, and the perception of environmental signals through ABA responses that include a transcription factor decay mechanism.

KEYWORDS

Arabidopsis thaliana, Autophagy, ABA signaling, bZIPs, ABI3, ABI5, Early imbibition, Protein storage vacuoles (PSV), Reserve mobilization, Seed germination.

INTRODUCTION

Autophagy, a conserved cellular mechanism in eukaryotic organisms, functions as a primary recycling system by degrading cytoplasmic components, thereby removing unnecessary and damaged cellular elements. Traditionally considered a non-selective bulk degradation mechanism, autophagy participates in the specific degradation of proteins, lipids, and organelles in response to biotic and abiotic stresses (Su *et al*., 2020; Qi *et al*., 2021). In plant cells, autophagy takes place in the central vacuole through vesicular trafficking processes such as macroautophagy and microautophagy. Macroautophagy is the most studied process and involves the transport of cargoes by a double-membrane vesicle known as the autophagosome, moving from the endoplasmic reticulum to the vacuole (Michaeli *et al*., 2016). In microautophagy, cytoplasmic elements such as lipid droplets (LD; also known as oil bodies and oleosomes), specialised organelles accumulating triacylglycerols (TAG) are directly engulfed by the central vacuole through tonoplast invagination (Siénko *et al*., 2020). Plant autophagy plays a crucial role in cellular homeostasis and facilitates adaptation to changing environments, making it essential for plant survival under various stresses and developmental programmes (Liu *et al*., 2009; Di Berardino *et al*., 2018).

In Arabidopis, the molecular machinery of autophagy comprises approximately 40 conserved proteins known as autophagy-related proteins (ATGs) and other evolutionary conserved factors related to autophagy. These proteins exhibit various functions and belong to more than seventeen protein families, such as kinases, ubiquitin-like proteins, vacuolar protein sorting factors and cysteine proteases (Ding *et al*., 2018). In *A. thaliana*, ATGs play a crucial role in three complexes associated with the formation of autophagosomes. Thus, (i) ATG1 kinase complex (ATG1, ATG11, ATG13, ATG101) regulates autophagy induction in response to nutrient starvation by interacting with the kinase Target Of Rapamycin (TOR) (Dobrenel *et al*., 2016); (ii) Phosphatidylinositol 3-kinase complex (PI3K: VPS15, VPS34, ATG6, ATG14) facilitates nucleation, that is, phagophore genesis (Yang *et al*., 2010); and (iii) the ATG complex, consisting of the proteins ATG9, ATG18 and ATG2, is crucial for recruiting membrane portions for the expansion of the phagophore (Sawa-Makarska *et al*., 2020). In autophagosome formation, the conjugating complex ATG8-ATG12 participates in two ubiquitin-like conjugation cascades critical for the attachment of phosphatidylethanolamine (PE) to the N-terminal of the ATG8 protein. The inner membranes of autophagosomes decorated withATG8-PE become crucial for the selective recruitment of autophagy cargo. This interaction occurs through ATG8-interacting motifs (AIMs), which engage receptor proteins such as the Neighbour of BRCA1 gene 1 (NBR1) and the translocator protein (TSPO) (Kellner *et al*., 2017; Ding *et al*., 2018; Luo *et al*., 2021).

The autophagy-related factors *AtATG5* and *AtATG7* are essential components of the autophagy machinery in both animals and plants (Xie and Klionsky, 2007; Minina *et al*., 2018; Fraiberg and Elazar, 2020). Genetic studies in *A. thaliana* described that *ATG* genes, specifically *ATG5* and *ATG7*, play a crucial role in the accumulation of storage proteins and lipids during embryogenesis and seed maturation (Fan *et al*., 2019). In Arabidopsis, overexpression of the *ATG5* and *ATG7* genes improves seed production and nitrogen content, and *atg5* and *atg7* mutants exhibit altered seed composition (Guiboileau *et al*., 2013; Masclaux-Daubresse *et al*., 2014; Di Berardino *et al*., 2018). Similarly, in *Oryza sativa*, autophagy affects starch quality, influencing both seed size and appearance, as *Osatg7-1* produces fewer and smaller seeds with a chalky appearance and a lower starch content in endosperm (Sera et al., 2019; Iglesias-Fernández and Vicente-Carbajosa, 2022).

Seeds play a crucial role in plant evolution, allowing plants to spread, endure adverse conditions, and resume growth in favourable environments (Finch-Savage and Bassel, 2016). The processes of seed maturation, germination, and post-germination, involve the accumulation and mobilisation of reserves, including starch, proteins (Seed storage proteins, SSP), and lipids (TAG) (Holdsworth *et al*., 2008; Bewley *et al*., 2013; Sajeev *et al*., 2024). The synthesis and storage of SSP in maturating seeds involves the endoplasmic reticulum. This cellular organelle facilitates the delivery of SSP to seed-specific vacuoles known as Protein Storage Vacuoles (PSV) through an autophagy-like process occurring both in the cotyledons and the embryonic axis (Hills, 2004; Vitale *et al*., 2022). Seed germination starts with water uptake and ends with endosperm rupture (ER) that allows radicle emergence (germination *sensu stricto*). The post-germination stages involve the hydrolysis of seed storage reserves by *de novo synthesised* proteases, providing essential support for seedling growth until the photosynthetic capacity is acquired (Nakabayashi *et al*., 2005). In imbibed Arabidopsis seeds, the degradation of SSP begins at the radicle, coinciding with cell expansion and differentiation. After radicle emergence (i.e. post-germination period), SSP catabolism occurs mainly in the cotyledons, especially when the SSP reserves of the embryonic axis are nearly depleted (Müntz, 2007; Iglesias-Fernández *et al*., 2014). In *Vigna mungo* (Fabaceae), the ERvt (Endoplasmic Reticule to vacuole trafficking) pathway has been reported to transport cysteine proteases from the endoplasmic reticulum to PSV, encapsulated within KDEL Vesicles (KV) (Okamoto *et al*., 2003). Interestingly, the autophagy receptor TSPO plays a major role in the regulation of fatty acids (FA) and LD in Arabidopsis germinating seeds and in seedlings. Recently, the mutant of LD structural protein - CALEOSIN 1 (CLO1) has been described to influence the degradation of LD by autophagy (lipophagy) in seeds germinating Arabidopsis (Jurkiewicz *et al*., 2018; Miklaszewska *et al*., 2023; Qin *et al*., 2023; Zhuang et al., 2024).

In the seedbed of natural soil, seeds face a complex environment with various stresses, requiring the development of molecular and cellular mechanisms for survival and adaptation. In this framework, seed vigour is determined by the capacity of seeds to germinate under a wide range of environmental conditions (Finch-Savage and Bassel, 2016). The endoplasmic reticulum in eukaryotes functions as a central organelle that detects and regulates stress responses. Under stress conditions, activation of the Unfolded Protein Response (UPR) pathway helps reduce the accumulation of unfolded proteins in the endoplasmic reticulum and restore cell homeostasis (Ellgaard *et al*., 2003; Yang *et al*., 2016). Stress persistence triggers the selective removal of specific endoplasmic reticulum domains through autophagy, as a feedback mechanism to alleviate protein overaccumulation (Stephani *et al*., 2020). Although autophagy is considered an important catabolic process involved in the specific degradation of cargoes in response to both biotic and abiotic stimuli, this process has not been thoroughly studied in seeds. In *Medicago truncatula*, endoplasmic reticulum stress and autophagy, mediated by MtATGs, play an important role in seed development and drought stress responses (Yang *et al*., 2021). Abscisic acid (ABA) is the main phytohormone that mediates the adaptation of the plant to abiotic stresses and controls seed maturation and dormancy. Furthermore, variations in the environment that can compromise embryo development result in the arrest of germination through an ABA-dependent mechanism during seed imbibition. In *A. thaliana*, the selective autophagy receptor NBR1 interacts with the transcription factors (TFs) ABA-Insensitive 3 (ABI3), ABI4, and ABI5, major regulators of ABA signaling, and overexpression of NBR1 decreases seed sensitivity to ABA (Carbonero *et al*., 2017; Tarnowski *et al*., 2020; Luo *et al*., 2021; Chen *et al*., 2022; Matilla, 2022).

In this study, we have explored the impact of autophagy on seed development through the characterization of *A. thaliana AtATG5* and *AtATG7* loss-of-function mutants. Homozygous seeds from Arabidopsis *atg5* and *atg7* knockout (KO) mutants germinate significantly slower than wild type (WT, Col-0), both under control conditions and when the imbibition medium contained ABA, a hormone that controls seed germination and mediates environmental stress signaling. Histochemical analysis of proteins and lipids demonstrated that these storage compounds showed alterations in mutants impaired in autophagy compared to mature WT seeds, both in the dry and imbibed stages. In particular, immunofluorescence labelling revealed the lack of localisation of the ATG8a protein in the PSV of *atg5* and *atg7* mutants, in support of the environment of an autophagy-like process in mobilisation of reserves to PSV.

A comprehensive transcriptomic analysis during germination in both *atg7* and Col-0 seeds revealed substantial transcriptional differences between dry seeds of *atg7* and Col-0 and at 96 hoi in the presence of ABA. In these conditions, approximately 10% of genes induced in *atg7* and repressed in WT ABA imbibed seeds have previously been reported as putative target genes for ABI3 and ABI5 TFs. We could confirm direct protein-protein interactions in yeast two-hybrid (Y2H) assays between ATG8 and both ABI3 and ABI5 TFs. Finally, Western blot experiments in autophagy mutants showed altered levels in key transcription factors involved in seed development such as ABI5 and bZIP67, supporting autophagy as a regulatory mechanism during seed maturation and imbibition. Taken together, our study highlights the role of autophagy as part of the seed development programme and its involvement in seed perception and response to environmental changes.

RESULTS

The *AtATG5* and *AtATG7* genes are expressed in embryos of *Arabidopsis thaliana* after seed development.

To study the impact of autophagy on seed development, a selection of 68 Arabidopsis thaliana autophagy genes was considered following a gene ontology (GO) classification (see Materials and Methods). Their expression patterns were analysed after retrieving comprehensive data from the public database of the Bio-Analytic Resource for Plant Biology (BAR) (https://bar.utoronto.ca/) to obtain a heatmap representation (Figure S1; Data S1). Taking into account the expression profiles obtained, we focus on *ATG5* and *ATG7,* as they are single-copy genes in Arabidopsis (*AtATG5*; locus *At5g17290*) and *ATG7* (*AtATG7*; locus *At5g45900*), which have been identified as essential components of the autophagy machinery in both animals and plants (Xie and Klionsky, 2007; Minina *et al*., 2018; Fraiberg and Elazar, 2020). Both genes showed high levels of expression during the late silique maturation and dry seed stages (DS) (Figure 1a).

We conducted a deeper examination of the spatial expression patterns of *AtATG5* and *AtATG7* using stable transgenic lines of *A. thaliana* (Col-0) bearing *AtATG5* and *AtATG7* promoters that drive GUS expression (described y Materials and Methods). Histochemical staining of these lines confirmed not only the ubiquitous expression of the *AtATG5* and *AtATG7* genes, but also their similar expression patterns. In both adult plants (75 days) and seedlings (15 days), GUS expression was observed in vascular elements of roots and leaves (Figure 1b and 1c). In addition, the expression of *AtATG5* and *AtATG7* was localised in pollen grains and in seeds at the late stages of silique maturation. In

seedlings, the expression of both genes was also found in the stem apical meristem (SAM) and slightly observed in cotyledons (Figure 1b and 1c).

Quantitative PCR (qPCR) was used to analyse the expression of the *AtATG5* and *AtATG7* genes during embryogenesis, seed maturation, and germination. The actin gene *AtACT7* was used as a reference gene, which showed stable expression throughout the period of study (Graeber *et al*., 2011; Figure S2). Figure 2 (a and b) shows gene expression levels throughout the early green (EG) to late green (LG) and brown (B) stages of silique development. *AtATG5* and *AtATG7* transcripts accumulate in the early stages of silique development (EG1 and EG2) and reach a maximum in the brown stage (late maturation stage (Figure 2b), consistent with the results shown in Figure 1. During seed germination, *AtATG5* and *AtATG7* mRNAs are highly detected in the stages of DS (Figure 2c), probably as a result of the accumulation of transcript during the late stages of silique maturation, followed by a sharp decrease in the early stages of imbibition (12 hoi) and a slight increase between 24-30 hoi, when the seeds reached t_{50} (time to get 50% seed germination). GUS histochemical staining was also analysed in germinating seeds of *PAtATG5::uidA* and *PAtATG7::uidA* transgenic lines. Figure 2d shows GUS staining at 24 and 48 hoi, where activity is specifically observed in the embryo and not in the endosperm. Upon seed imbibition, GUS activity was initially observed in the reporter lines in the radicle transition zone of the embryonic axis at 24 hoi. Subsequently, at 48 hoi, the signal expanded to both the hypocotyl and the cotyledons, where the intensity increased as they expanded (Figure 2c). Collectively, the expression data obtained are consistent with the participation of *AtATG5* and *AtATG7* during seed development in both the maturation and germination phases.

Seed germination in *atg5* and *atg7* knockout mutants is impaired and significantly delayed in the presence of ABA during imbibition.

Taking into account the expression patterns of the *AtATG5* and *AtATG7* genes observed in the embryo during seed imbibition, we set out to investigate their relevance in the germination process of Arabidopsis seeds. We used homozygous T-DNA insertion mutant lines *atg5-1* and *atg7-2* (Hofius *et al*., 2009; Yoshimoto *et al*., 2009; Avin-Wittenberg *et al*., 2015; Barros *et al*., 2017; Erlichman *et al*., 2023), to assess the influence of the *AtATG5* and *AtATG7* genes on germination under both control conditions and in the presence of 1 µM ABA in the imbibition medium. ABA is known to play a crucial role in germination by regulating the transition from dormancy to active growth, and we used the ABA-insensitive *abi5-7* mutant as a negative control for ABA responsiveness. The lack of *AtATG5* and *AtATG7* transcripts in the *atg5*, and *atg7* mutant lines was confirmed by qPCR, while *abi5-7* showed some leaky basal expression (Figure S3).

Seed Coat Rupture (SCR) and Endosperm Rupture (ER) were scored in Col-0, *atg5* and *atg7* KO mutant lines (Figure 3). Under control conditions, the *atg5*, *atg7*, and *abi5-7* mutants showed a noticeable and significant delay in germination, evidenced by an increase in t_{50} for both SCR and ER parameters compared to Col-0 (Figure 3). Although the presence of 1 µM ABA had a faint effect on Col-0 and *abi5-7* SCR, a significant delay in ER was observed for *atg5* and *atg7*, and these mutants did not reach t_{50} within the observed period. On the contrary, Col-0 seeds achieve t_{50} at 69.3 ± 4.2 h. and *abi5-7* seeds exhibited reduced sensitivity to ABA, as expected, and achieved t_{50} at 55.6 ± 1.2 h.

Analysis of *PAtATG5:: uidA* and *PAtATG7:: uidA* imbibed seeds showed that spatial expression and intensity of GUS activity were not significantly modified in the presence of 1 µM ABA, compared to control conditions (Figure S4a). Similarly, quantifying the expression of the *AtATG5* and *AtATG7*

gene by qPCR in the presence of ABA in imbibition medium yielded results similar to the expression levels observed under control conditions (Figure S4b).

Comprehensive transcriptomic profiling of *Arabidopsis thaliana atg7* during seed imbibition reveals important changes in gene expression in the autophagy mutant

To study transcriptional changes during seed germination in Col-0 and *atg7*, both in the absence and presence of 1 µM ABA, we performed RNA-seq analysis on dry and imbibed seeds, collected at 0, 24, 48, and 96 hoi (experimental design depicted in Figure S5a). These time points cover t_0, t_{25}, t_{75}, and t_{100} (time to obtain 100% germination; Figure S5a). At designated time points, total RNA was extracted and, after library construction, RNA sequencing analysis was performed.

A general survey of the entire data set was performed to assess the quality and consistency of the samples by clustering and principal component analysis (PCA). As disclosed by PCA, the highest expression variance was observed between the *atg7* and Col-0 samples after 24 hoi (Figure S5c), while little variance was detected between the equivalent samples of DS. Samples from imbibed seeds of *atg7* and Col-0 at 48 hoi under control conditions, and 96 hoi in the presence of ABA (1 µM) showed slight variance differences. Similar results were also obtained in the cluster analysis (Figure S5b). The samples were clustered first by biological triplicates and second by time points of imbibition, and most differences were again found between Col-0 and *atg7* samples at 24 hoi under control conditions.

From our results obtained by PCA and clustering analyses, the comparison between Col-0 and *atg7* at 24 hoi in control conditions was chosen for the subsequent study of differentially expressed genes (DEG; Data S2). Figure 4a shows the volcano plot from a differential gene expression analysis under restrictive thresholds (Log_2FC; cut-off ≤ 2.0) an adjusted *p*-value ≤ 0.05). Among the DEG with significant values that show higher expression in the *atg7* mutant compared to the WT, there were important genes associated with the synthesis and mobilisation of storage compounds (see Figure 4a for individual examples within the volcano plot). Gene set enrichment analysis (GSEA, *p*-value = 0.05) was carried out on Col-0 and *atg7* mutant at 24 hoi in control conditions by ranking genes according to Log_2FC. The analysis showed that 9 induced and 6 repressed pathways were identified as significantly enriched categories (Figure 4b; Data S3). GO (Biological Process; BP) categories such as lipid storage and seed maturation are over-represented within induced genes, while the response to the endoplasmic reticulum stress category, which includes autophagy, was detected among repressed ones (Figure 4b). In Figure 4c, heatmaps illustrate the Log_2FC of genes within distinct categories, including lipid storage (n= 9 genes), seed maturation (n = 11 genes), and response to endoplasmic reticulum stress (n= 8 genes) (Data S3). The genes involved in seed maturation include *AtCRC (CRU3*), *AtCRA1* (12S SSP, cruciferins), and *AtCLO1* and *SEIPIN1* (lipid storage-related genes). *AtCLO1* encodes a 27 kDa caleosin protein located within the lipid bodies of seeds, while *SEIPIN1* encodes a membrane protein primarily involved in LD biogenesis, particularly in embryos. Furthermore, in the category of lipid storage, three genes were present, OLE1, *OLE2*, and *OLE3, encoding oleosins.* These proteins, found in oil bodies, play a pivotal role in the accumulation of lipids in seeds. Notably, lipid storage is associated with three Late Embryogenesis Abundant (LEA) protein-encoding genes *SSLEA*, *LEA29*, and *LEA7.* Interestingly, three aquaporin-encoding genes (Tonoplast intrinsic protein; TIP), including *TIP3;1* (*ALPHA-TIP*; *At1g73190*), were differentially expressed. *TIP3;1* encodes an aquaporin located in the tonoplast, specifically within PSV in embryos. As illustrated in Figure S1, the *TIP3;1* gene stands out as the most expressed autophagy-related

protein in seeds. Since autophagy is activated in endoplasmic reticulum stress, genes implicated in this response exhibit decreased expression in the mutant compared to the WT, as expected. Notably, the repressed genes include *Binding Protein 3* (*BIP3*) and *Inositol Requiring 1* (*IRE1C*). BIP3 encodes a member of the HSP70 family of UPR-induced heat shock proteins, and IRE1C represents an isoform of IRE1A and IRE1B, which are endoribonuclease/protein kinase proteins involved in UPR in the endoplasmic reticulum (Figure 4c). These findings suggest that autophagy is involved in lipid and protein metabolism during early seed imbibition.

Histochemical analysis of protein and lipids in *atg* mutants during seed imbibition reveals autophagy-related changes in the accumulation and dynamics of storage compounds.

The transcriptomic analysis described above revealed a significant upregulation of genes associated with storage compounds in imbibed seeds of the *atg7* mutant compared to the WT (Figure 4). To further investigate this finding, the detection of seed lipids and proteins was carried out in both *atg5* and *atg7* mutants, as well as in the WT, at 24 and 48 hoi.

Microscopic examination of embryos using Nile red for lipid staining (Figure 5) demonstrated similar levels in *atg5* and *atg7* mutants and Col-0 at 24 hoi (Figure 5a). However, a quantitative analysis of the percentage of lipid /cell area in the radicle region for each line at 48 hoi (Figure 5b) showed that the percentage of lipid/cell area is significantly lower in mutants (*ca.* 30%) than in WT (ca. 45%).

Likewise, GO analyses revealed differences when *atg7* was compared with WT in the category of genes related to seed maturation proteins. Examples include *AtCRC* (*CRU3*) and *AtCRA1*, which encode 12S-SSP (cruciferins), highly abundant SSP in seeds of *A. thaliana.* These proteins accumulate in PSV during seed maturation. To investigate SSP in Col-0, *atg5*, and *atg7* seeds, in DS and imbibed satages, a histochemical analysis was performed. Longitudinal sections of *A. thaliana* seeds (DS and water-imbibed at 24 and 48 hoi) were stained using Periodic acid–Schiff (PAS) and Naphthol Blue Black to detect insoluble polysaccharides (mainly cellulose and starch) and proteins, respectively. As shown in Figure 6a–f, both DS and imbibed seeds exhibited abundant proteins (blue stained). In Col-0 DS, proteins accumulated within well-defined PSV represented by rounded structures (Figure 6a-b). On the contrary, although both *atg5* and *atg7* DS are rich in proteins, their cytoplasm showed altered organisation, especially in the radicle (Figure 6a-r). These differences in cytoplasmic organisation, relative to protein accumulation in radicle cells of *atg* mutants, persist at 24 hoi (Figure 6g-l). At 48 hoi, proteins were completely degraded in both Col-0 and mutants after radicle emergence (Figure 6m–r).

Immunolocalization of the ATG8 protein in wild-tpe but not in *atg* mutant PSVs supports an autophagy-like mechanism involved in reserve mobilisation during seed development.

The insights presented above from genetic, transcriptomic, and histochemical analyses during seed imbibition and reserve mobilisation prompted us to explore the molecular link between storage compound mobilisation and autophagy. To this end, we performed immunofluorescence labeling using a primary antibody specific to ATG8a protein (Miklaszewska *et al*., 2023) participating in autophagosome capture of cargoes (Figure 7a-l, Figure S7). The presence of the ATG8a protein was detected in longitudinal sections of Col-0 seeds imbibed at 24 hoi. As illustrated in Figures 7a-c, ATG8a is predominantly localised within PSVs in the radicle of Col-0 seeds. Interestingly, this localisation was absent in *atg5* and *atg7* embryos (Figure 7e-g, i-k). Secondary/primary antibodies and empty negative controls did not show fluorescence signals as expected (Figures S7a-i).

Examining coarse sections (8 µm) of paraffin samples through differential interference contrast (DIC) microscopic analysis revealed that the cellular organisation of seed tissues had been well preserved (Figure 7d, h, l; Figure S7c, f, i). Although these data do not rule out the presence of other ATG8 proteins in PSVs in the radicle of *atg5* and *atg7* embryos, our histochemical assays support the participation of autophagy not only in lipid and protein metabolism, as suggested by our transcriptomic data, but also in its cytoplasmic organisation of embryo cells throughout seed development.

Transcriptomic profiling of *atg7* imbibed seeds reveals a connection of autophagy to ABA responses and genes regulated by ABI3/ABI5.

ABA is a well-known hormone that regulates seed development and germination. The autophagy mutants studied showed a delayed germination phenotype compared to the WT seeds, especially manifested in the presence of 1 µM ABA during imbibition (Figure 4). To further explore the molecular basis of ABA responses in the *atg7* mutant, we focus on the precise stages of our comprehensive transcriptomic approach. We compared transcriptional differences during seed imbibition in the absence and in the presence of ABA between Col-0 and the *atg7* mutant (Figure S5). To examine the particular effects of ABA independently of the seed development stages, we decided to compare the transcriptomes of the germinating seeds *atg7* and Col-0 under two conditions: 96 hoi in the presence of ABA (hereafter 96-ABA hoi) and 48 hoi in the absence of ABA (48 hoi) since they represent time points where seeds achieve similar germination rates and comparable physiological stages (Figures 4 and S5). Hence, the DEG comparison was performed by contrasting data obtained from Col-0 and *atg7* imbibed seeds at 96-ABA hoi against 48 hoi in each line (Data S4 and S5). DEG analysis was performed with cut-offs of p-adj. ≤ 0.05 and $\log_2 FC \geq 2$. Consequently, in Col-0, 607 induced genes and 890 repressed genes were identified in response to ABA during seed imbibition (Figure 8a; Data S6), while in *atg7*, a set of 636 induced genes and 838 repressed genes were found in response to ABA. Interestingly, upon comparison using a Venn diagram, it was observed that among the four gene lists (Col-0 induced, Col-0 repressed, *atg7* induced, and *atg7* repressed), 333 genes were induced in Col-0 and repressed in the *atg7* mutant, while 443 genes were induced in *atg7* and repressed in Col-0 seeds (Figure 8a). To gain further insight into the specific biological processes influenced by ABA-autophagy crosstalk in the *atg7* mutant, GO analysis was carried out independently in the two groups of genes: those induced (n=443 genes) and those repressed (n=333 genes) in the *atg7* mutant, showing opposite expression patterns compared to WT (Figure 8b; Data S7, heatmap). The analysis revealed a notable enrichment of genes related to cell wall modification and organization GO terms in the *atg7*-repressed gene list (Figure 8b-top panel, Data S7, enrichment down). On the contrary, significant enrichment of genes associated with seed oil biogenesis, lipid storage, seed maturation, and stress response GO terms, particularly in the ABA response category, was observed in the *atg7*-induced gene list (Figure 8b-bottom panel, Data S7, enrichment up). The opposite transcriptional response to ABA was observed in a set of genes in the autophagy-deficient mutant compared to the WT, suggesting a connection between ABA responses and autophagy during seed imbibition.

Among the set of DEGs discovered in the formerly described transcriptomic analysis, 48 of the 433 genes induced in the *atg7* mutant and repressed in WT imbibed seeds have previously been reported as putative target genes for ABI3 and ABI5 TFs (Figure 8c; Data S8). Moreover, 10 of the 48 genes were classified in the ABA response category (Figure 8c). ABI3 is a B3 TF, which acts together with ABI5 bZIP TF, as master regulators in the complex network of ABA signaling cascades within seeds.

They are important seed-specific downstream ABA targets and are considered repressors of germination (Sajeev *et al*., 2024). The expression patterns of these 48 genes in siliques and seeds were examined using the Gene Expression Tool available in the public database of the Bio-Analytic Resource for Plant Biology (BAR) (https://bar.utoronto.ca/). A heatmap representation of the expression data revealed that 33 genes exhibited high levels of expression in the late stages of seed maturation, as well as in DS (Figure 8c).

The autophagy protein ATG8 interacts directly with ABI3 and ABI5 transcription factors and supports their autophagy-mediated modulation.

The transcriptomic analysis previously described suggested the relevance of the ABI3 and ABI5 factors in relation to autophagy during seed development. Sequence analysis of the ABI3 and ABI5 proteins revealed that they contain 6 and 5 potential ATG8 AIMs, respectively (Figure S8). Taking this information into account, we decided to explore their association with autophagy machinery and verify whether ABI3 and ABI5 could interact *in vivo* with ATG8 using Y2H assays (Figure 9a). To test this possibility, we fused the coding sequence of the ATG8H protein, the major *ATG8* gene expressed during seed germination (https://bar.utoronto.ca/), to the GAL4 DNA binding domain and used it as bait. Yeast cells that carried the BD-ATG8H and the AD-ABI3 and AD-ABI5 constructs, but not those that harbored the control plasmids or the AD-ATG8H construct, were able to grow in selective medium in the presence of concentrations of 3-aminotriazole (3-AT) higher than 60 mM, indicating that ABI3 and ABI5 can interact with the ATG8 protein (Figure 9a).

To deepen our findings linking these TFs with the autophagy machinery, we focused on ABI5, a bZIP TF primarily expressed in seeds and associated with suppression of germination and post-germination growth under adverse conditions (López-Molina *et al*., 2001; Albertos *et al*., 2015). ABI5 accumulation was systematically monitored in the *atg5* and *atg7* mutants, both in the DS and during imbibition, compared to the WT seeds. Western blot assays were performed at 0, 36, 48, and 72 hoi using a primary antibody specific for the ABI5 protein (Figure 9b). The signal intensities of the Western blot assays were quantified using ImageJ software and plotted in Figure 9c. This figure shows that ABI5 is clearly detected in WT seeds in DS (0 hoi) but shows increased levels in autophagy mutants *atg5* (nearly 2-fold) and *atg7* (about 2.5-fold) This difference in ABI5 accumulation was further monitored at different time points during imbibition (see Figures 9b and 9c) where it shows a temporal decline until untraceable levels around 72 hoi. These findings indicate that autophagy can play an important role in modulating ABI5 accumulation during seed imbibition. Furthermore, we verified that another bZIP factor expressed in the seed, bZIP67, the closest homolog ABI5 described as a regulator of omega-3 FA content in Arabidopsis seeds (Mendes *et al*., 2013; Sánchez-Vicente et al., 2024), also accumulates to a greater extent in autophagy mutants *atg5* and *atg7* and shows decreased levels in *ATG5* and *ATG7* overexpression lines (Figure S9a). The bZIP67 protein also contains three putative AIMs (see Figure S9b). Interestingly, genes such as *cruciferin 1* (*CRU1*), *CRU2*, *CRU3*, *seed storage albumin 1* (AT2S1) and *fatty acid elongation 1* (*FAE1*), previously recognised as bZIP76 target genes with roles in protein and lipid metabolism in seeds (Mendes *et al*., 2013), were induced by ABA in *atg7*-imbibed seeds compared to Col-0, as revealed by our transcriptomic analysis (refer to Figure S9c).

DISCUSSION

In recent years, autophagy has been increasingly linked to a diverse array of plant biological processes, including development, nutrient recycling, and responses to both abiotic and biotic stresses. Although several studies have acknowledged its role in seed development (e.g., Michaeli et al. 2016; Tarnowski et al., 2020), the molecular mechanisms and targets involved remain partially understood. In this work, our aim was to explore its impact on seed germination in *Arabidopsis thaliana* through the study of autophagy mutants *atg5* and *atg7* with a special focus on their connections to ABA signaling.

Autophagy mutants *atg5* and *atg7* show a delayed seed germination phenotype and hipersensitivity to abscisic acid

AtATG5 and *AtATG7* are single copy genes in the Arabidopsis genome, whose gain- and loss of function mutants have been successfully used to unveil different autophagy-related phenotypes (Hofius *et al*., 2009; Yoshimoto *et al*., 2009; Ohlsson *et al*., 2023). As a first step in studying their possible involvement in germination, we performed a detailed examination of their spatial and temporal gene expression patterns, especially during seed development.

Transcriptomic data retrieved from the BAR public database showed high expression levels of both genes in dry seeds, early imbibed seeds, late stages of silique maturation, and mature pollen. These results were confirmed by qPCR and extended in our spatial expression analysis, conducted using GUS histochemical staining (Figure 1 and 2). The expression driven by the *ATG5* and *ATG7* promoters was observed in the vascular elements of roots and leaves, mature pollen grains and seeds in the late stages of silique maturation, as described in previous reports in Arabidopsis and other species such as maize (Thompson *et al*., 2005; Li *et al*., 2015; Yu and Hua, 2022). We also found clear expression of *AtATG5* and *AtATG7* in the stem apical meristem and to a lesser extent in seedling cotyledons. Our observations of *AtATG5* and *AtATG7* expression in mature pollen grains and vascular elements are fully in agreement with previous published reports. Autophagy has been associated with stress-induced microspore embryogenesis in Brassicaceae (*A. thaliana* and *Brassica napus*), and more specifically *AtATG5* and *AtATG7* are involved in the regulation of pollen germination, tube growth guidance, and sperm cell development (Yan *et al*., 2023; Testillano, 2019; Berenguer *et al*., 2021). Furthermore, it has been recently described as a universal mechanism that participates in the formation of both tracheary elements (dead tissues; xylem) and sieve elements (alive tissues; phloem; Michalak *et al*., 2024).

Likewise, in the context of the seed our results support previous work reporting that expression of almost all the *A. thaliana ATG* genes increases during seed development, especially during maturation (Di Berardino *et al*., 2018; Bedu *et al*., 2020), and that seeds of *atg5* and *atg7* exhibit a reduced nitrogen content possibly due to a defective remobilization (source: sink ratio) of this macronutrient. Furthermore, evolutionary conservation of the function of ATG was reported in different plant species like *M. truncatula* (Fabaceae), where *MtATG* transcripts are also highly induced during the late stages of seed maturation, and in monocot *Zea mays*, suggesting that autophagy could participate in the maturation and death of the endosperm during seed development, having an impact on seed production and yield (Guiboileau *et al*., 2012; Li *et al*., 2015; Barros *et al*., 2017; Minina *et al*., 2018; Sera *et al*., 2019; Liu et al., 2023).

Interestingly, *AtATG5* and *AtATG7* expression peaks in the late stages of seed maturation (LG2 and Brown; Figure 2a) matching with ABA increase, the synthesis of storage compounds (proteins and lipids) and the induction of primary dormancy (Ali *et al*., 2021). These results led us to investigate the germination capacity of *atg5* and *atg7* seeds. When we performed germination assays, we observed a significant delay in germination in knockout mutants *atg5* and *atg7* compared to WT under control conditions and most conspicuously in the presence of ABA.

Slower germination of the *atg* mutants was reflected by the increase in t_{50} of both SCR and ER parameters (see Figure 3). In germinating transgenic seeds expressing *uidA* reporter under the control *AtATG5* and *AtATG7* gene promoters, GUS activity is mainly found in the radicle transition zone of the embryonic axis at 24 hoi, especially that of *AtATG7*. Subsequently, at 48 hoi, the signal extends to both the hypocotyl and cotyledons. This spatiotemporal pattern resembles the dynamic model for reserve mobilisation that involves SSP hydrolysis at the PSV first on the embryonic axis until exhausted, and then at the cotyledons (Müntz, 2007; Iglesias-Fernández *et al*. 2014). These results suggest that *AtATG5* and *AtATG7* might affect germination *sensu stricto* by controlling storage mobilization in the radicle. Interestingly, while the *atg5* and *atg7* mutant seeds germinate slower than those of the WT, the F1 seeds from maternal *atg mutant* plants show earlier germination, possibly due to increased water permeability combined with normal autophagy in the embryo. Seeds from maternal *atg* mutants showed reduced mucilage content and experienced structural changes at both the cellular and general organ levels, as indicated by seed coat analysis (Erlichman *et al*., 2023).

Notably, in the presence of ABA, *atg5* and *atg7* have even a slower germination rate than WT seeds. However, the spatiotemporal expression of *AtATG5* and *AtATG7* is not altered when ABA is present in the seed imbibition medium (Figure S4), suggesting that ABA does not influence their expression but induces changes in other factors that affect germination. Altogether, our data suggest a role for autophagy not only in the progression of seed germination under non-stress conditions but also in response to environmental changes, particularly involving ABA signaling, as observed by the addition of ABA during seed imbibition.

Transcriptomic analysis and reserve mobilisation in *atg7* mutant seeds during imbibition

We have compared the transcriptomes of wild-type seeds and the *atg7* mutant during early seed imbibition (24 hoi) to uncover major changes related to autophagy. We unveiled significant transcriptional changes when we analysed the DEGs (see the Results section for detailed gene lists) and found GO enrichment in processes associated with storage compounds, mainly lipids and proteins. Hence, we performed detailed histochemical analyses of protein bodies and lipid droplets in mature dry seeds and after imbibition when storage compounds were mobilised.

Oilseed plants such as *A. thaliana* store lipids mainly as TAG in lipid droplets (LD), which consist of a neutral lipid core surrounded by a phospholipid monolayer containing specific proteins such as oleosins and caleosins (Miklaszewska et al., 2023). In Arabidopsis, the seed-specific oleosins AtOLE1 and AtOLE2 are the main proteins involved in the formation and degradation of LD (Simada et al., 2008; Chen et al., 2019; Shao et al., 2019). We observe that *atg7* germinating seeds (24 hoi) express higher levels of *AtOLE1*, *AtOLE2* and *AtOLE3* than WT, suggesting a mechanism to compensate for the impairment of lipid turnover in this mutant. Interestingly, both ectopic overexpression and suppression of oleosin cause a delay in germination in Arabidopsis seeds, supporting the involvement of oleosins in the regular course of seed germination (Siloto et al., 2006; Yuan et al., 2021). In addition to oleosins, *AtSEIPIN* and caleosin *AtCLO1* are among the DEGs detected in the *atg7* and

WT profiles during seed imbibition. *AtSEIPIN* encodes an endoplasmic reticulum membrane protein exclusive to developing embryos that is involved in the biogenesis of LD (Zhao et al., 2023). *AtCLO1* is expressed exclusively during seed development and has also been implicated in LD degradation (Naested et al. 2000; Kim et al., 2011). Furthermore, Arabidopsis *clo1* KO mutants show a delay in the breakdown of storage lipids in germinating embryos, and CLO1 has also been involved in the LD-vacuole interaction during germination (Poxleitner et al., 2006). Protein-protein interactions have been demonstrated between AtATG8 and AtCLO1, and AtATG8 and AtOLE1 through AIMs. Furthermore, AtATG8 colocalizes with LD during seed germination, which are engulfed by the tonoplast through a microlipophagy-like process (Marshall et al., 2019; Miklaszewska et al., 2023). Induction of genes encoding LD structural proteins in the *atg7* mutant during germination supports the participation of autophagy in both lipid seed content and the cellular mechanisms that govern the dynamics of LD.

Previous studies in several autophagy mutant lines have established alterations in lipid content. Arabidopsis knockout mutants in the *ATG2*, *ATG5* and *ATG7* genes showed a lower content of lipids (i.e. TAG and FA) in seeds (Minina et al., 2018). Fan et al. (2019) demonstrated, using short-term ^{14}C-acetate and ^{3H2O} labelling, that reduced TAG levels in *atg2* and *atg5* mutants are not caused by a reduction in FA synthesis rate but result from an impairment of membrane lipid recycling. Similarly, Havé et al. (2019) detected a higher accumulation of phospholipids and sphingolipids in *atg5* compared to WT, influencing the composition of the endoplasmic reticulum and the plasma membrane. Our results contained in Figure 5 are in line with these observations. Histochemical detection of lipid droplets in *atg7* mutant seeds did not show significant differences from wild type upon imbibition at 24 hours. Nevertheless, they present altered lipid mobilization as reflected by a faster degradation observed in *atg7* seeds at 48 hoi. Altogether, these data underline the role of autophagy in lipid mobilization upon early seed germination.

Arabidopsis seeds contain two main classes of seed storage proteins, 12S globulins (cruciferins) and 2S albumins (napins) stored in PSV, which are mobilised upon seed imbibition (Baud *et al*., 2008). In our transcriptomic analysis, higher levels of the *AtCRU1* and *AtCRU3 cruciferin genes* are present during early imbibition in the *atg7* mutant compared to WT. In histochemical analysis of seeds at the stages of DS and 24 hoi, we observe alterations in PSV organisation in radicle cells in *atg5* and *atg7* mutants compared to WT. These differences disappear after the emergence of the radicle (48 hoi). The disorganisation detected in the PSV of dry seeds of *atg* mutants supports the notion of a mechanism of mobilisation of seed storage proteins to protein storage vacuoles through an autophagy-like ERvt mechanism (endoplasmic reticulum vacuole trafficking) mechanism (Hills, 2004; Vitale *et al*., 2022). Furthermore, immunolocalization assays of the ATG8 protein in germinating seeds (24 hoi) restrict the localisation of ATG8 to PSV in Col-0. On the contrary, ATG8 is not detected in *atg5* and *atg7* at 24 hoi, indicating that impaired autophagy affects cell vesicle trafficking and degradation in the embryonic axis during germination. Interestingly, *TIP3;1* and *TIP3;2,* encoding seed-specific aquaporins in the tonoplast of the PSV, are among the most induced genes in the *atg7* mutant compared to the WT. These genes are highly expressed during seed maturation and early germination and have been reported to modulate ABA responses (Maurel et al., 2015). Our transcriptomic analysis revealed the presence of other genes upregulated in *atg7* that have been involved in ABA responses, encoding LEA proteins such as AtEM6, AtSSLEA, AtLEA29, and AtLEA7 (Zhang et al., 2008, Huang et al., 2018) and *DOG1* (Delay of germination-1), a master regulator of primary seed dormancy and in controlling the timing of germination (Bentsink et al., 2006; Carrillo-Barral et al., 2020). Altogether, the accumulation in *atg7* of transcripts of ABA-responsive genes such as *LEA, TIP,* and *DOG1* can

contribute to the delayed germination phenotype observed in this mutant, suggesting a role for autophagy in mediating ABA response in seed dormancy and early imbibition.

A connection of the delayed germination phenotype and ABA responses to the stability of the ABI5 protein in the *atg7* mutant

ABA is a key phytohormone in the control of seed maturation and dormancy, which also regulates abiotic and biotic stress responses. We have shown that the *atg5* and *atg7* mutants exhibit a delay in germination (Figure 3), particularly evident when germinated in the presence of ABA. Furthermore, our comparative analysis of the transcriptomes of *atg7* and Col-0 in the presence and absence of ABA reveals opposite expression patterns in equivalent developmental stages (96 hoi in the presence of ABA and 48 hoi in the absence of ABA), where the GO ABA response category is significantly overrepresented among the induced genes in *atg7*. Notably, our transcriptomic analysis shows that approximately 10% of the genes induced in *atg7* and repressed in Col-0 in the presence of ABA are putative target genes for ABI3 and ABI5, suggesting that ABA signaling in *atg7* is altered.

ABI3 and ABI5 are important seed-specific downstream ABA targets that suppress germination in orthodox seeds and regulate preharvest sprouting (Koornneef *et al*. 1984; Finkelstein 1994; Abraham *et al*., 2016; Matilla, 2022; Sajeev *et al*. 2024). ABA regulates the progression of seed germination in response to changes in the environment (López-Molina *et al*., 2001). An important connection between abscisic acid signaling and autophagy has been described through the selective autophagy receptor NBR1, essential to fine-tuning ABA signaling, and its physical interaction with ABI3, ABI4, and ABI5 (Tarnowski *et al*., 2020). These factors have also been identified in proteomic analyses of proteins immunoprecipitated with antibodies specific for the autophagy factor ATG8 (Dagdas Y, personal communication). In our study we have further investigated these interactions to validate that ABI3 and ABI5 can interact directly with ATG8 in Y2H assays (Figure 9), in support of the possibility that these TFs could be degraded by autophagy. Furthermore, we have demonstrated progressive decay of ABI5 during seed germination, in a profile compatible with ATG8-mediated degradation by autophagy (Figure 9). Consequently, ABI5 degradation in germinating seeds occurs slower in *atg5* and *atg7* compared to WT, supporting the observed ABA hypersensitivity and delayed germination phenotype. Interestingly, not only is ABI5 abundance controlled by autophagy during germination, but also the levels of its closest relative bZIP transcription factor bZIP67 are altered in *atg7* mutants (Figure S9). Specifically, putative target genes for bZIP67 (*CRU1, CRU2, CRU3, AT2S1, FAE1*) show an induction of their expression in the *atg7* mutant (Mendes *et al*., 2013; Figure S9). These data suggest that bZIP67 protein levels are controlled by autophagy upon seed maturation. In conclusion, our results highlight that autophagy may serve as a broad mechanism controlling how germinating seeds respond rapidly to environmental changes. This mechanism would imply control of the protein levels of selected TFs involved in specific environmental responses.

Conclusions

The data presented here highlight the role of autophagy not only in the accumulation of reserves during seed maturation but also in the mobilisation of storage compounds during early seed imbibition in *A. thaliana*. Our findings support the role of autophagy in cell vesicle trafficking in the radicle, contributing to the cellular dynamics of LD (lipid turnover) and PSV (protein storage and mobilisation). Our findings also indicate a role for autophagy in mediating the ABA response during early imbibition. This response involves the regulation of protein levels of selected TFs, such as ABI3 and

ABI5, which are pivotal in specific environmental responses. Consequently, autophagy emerges as a broad mechanism that controls how germinating seeds respond rapidly to environmental cues (Figure 10). Therefore, autophagy likely plays a crucial role in the seed development programme and seed environmental perception (seed vigour) in *A. thaliana*. However, the question of whether these processes in *A. thaliana* can be extrapolated to other dicotyledonous species or even monocotyledonous species, with different seed anatomy and storage compounds, needs further investigation. Our work sheds light on seed autophagy and its fundamental importance in enhancing plant yield. Targeting autophagy genes associated with high seed yield and vigour will be crucial to achieving this goal.

EXPERIMENTAL PROCEDURES

Plant material and growth conditions

Arabidopsis thaliana Columbia (Col-0) ecotype was used as WT. Knockout T-DNA insertion lines were used for *ATG5* (*atg5-1;* SAIL_129B079) and *ATG7* (*atg7-2;* GK-655B06; Hofius *et al*., 2009; Yoshimoto *et al*., 2009), kindly donated by C. Masclaux-Daubresse (IJPB, France) and *ABI5* (*abi5-7*; Albertos *et al*., 2015).

Seeds were surface sterilized in 70% ethanol for 15 min followed by a 100% ethanol wash, and then air dried. Next, they were plated on solid half-strength basal Murashige and Skoog medium including vitamins supplemented with 1% sucrose (MS/2; Duchefa Biochemie, Haarlem, Netherlands) and then stratified for 3 d at 4ºC. Seeds were kept for 2 weeks at 21ºC in a germination chamber with a light intensity of 155 µmol photons/m^2/s under a long-day photoperiod (16h/8h; day/night). Seedlings were transferred to soil: vermiculite (3:1) pots and grew in a greenhouse under similar conditions. Siliques were collected to recover seeds at different seed embryogenesis and maturation stages for RNA isolation. The remaining mature brown seeds were harvested and stored at 21ºC and 30% relative humidity, until used. After one month under these conditions, mature seeds were considered after-ripened.

Germination assays

Three replicates of 50 after-ripened mature seeds were sterilized as above and subsequently imbibed on moist nitrocellulose filter papers (Whatman nº1; Thermo Fisher Scientific; Waltham, MA, USA) placed on 55 mm Petri dishes containing solid MS/2 with or without 1 µM 2-cis, 4-trans-Abscisic acid (ABA; Merck, Rahway, NY, USA). Plates were kept in a germination chamber in the above conditions.

The Seed Coat Rupture (SCR) and Endosperm Rupture (ER) were evaluated at 0, 24, 30, 36, 48, 54, 72, 76, and 80 hoi under an Olympus stereo microscope SZ2-ILST (Olympus; Tokyo, Japan). Statistical analysis and the time to get the 50% germination (t50) were calculated using the GERMINATOR Microsoft Office Excel 16.9 package (Joosen et al., 2010).

Col-0 and atg7 imbibed seeds were also collected at selected time points (0, 24, 48, 96 hoi in the absence and presence of 1 µM ABA) and frozen in liquid nitrogen for RNA isolation and subsequent RNA-seq analysis.

Generation of PAtATG5::uidA and PAtATG7::uidA transgenic lines and histochemical GUS assays

AtATG5 (At5g17290) and AtATG7 (At5g45900) native promoter sequences were amplified from A. thaliana genomic DNA (from -396 bp and -339 bp before the initial ATG, respectively), using

oligonucleotides containing BamHI and SalI restriction enzyme sites (Table S1). PCR products were cloned into the pGEM T-easy vector (Thermo Fisher Scientific) according to the manufacturer's instructions and then transferred into the pBI101 vector (between BamHI and SalI sites), containing the Escherichia coli uidA reporter gene. Recombinant plasmids were used to transform C51C1 Agrobacterium tumefaciens cells by electroporation using an ECM 630 Electroporator (BTX; Harvard Bioscience, Holliston, MA, USA) and then introduced into A. thaliana Col-0 plants using Agrobacterium floral dip transformation (Clough and Bent, 1998). The presence of the pBI101 vector in T1 generation was identified based on their hygromycin resistance (40 mg/L). Selected plants from the subsequent generations were allowed to self-fertilize until homozygous lines were identified in the T3 generation, showing 100% germination in the selection media.

AtATG5 and AtATG7 native promoter space-time expression was evaluated in a representative transgenic line out of 10-12 independent homozygous lines by qualitative GUS staining (Jefferson et al., 1987) and visualized under a Leica DMi8 light microscope (Leica, Wetzlar, Germany).

RNA isolation, cDNA synthesis, and quantitative PCR assays (qPCR)

Total RNA was purified from Col-0, atg5, and atg7 as described (Oñate-Sánchez and Vicente-Carbajosa, 2008) at different germination time points (0, 12, 24, 30, 36, 42 hoi) and different stages of seed embryogenesis and maturation: early green seeds (EG, <7 mm) late green seeds (LG, 7-10 mm) and brown seeds (B, >10 mm, with brown color). The quality and concentration of isolated RNA were tested by absorbance analysis using a Nanodrop® ND-1000 spectrophotometer (Thermo Fisher Scientific).

cDNA was synthesized from 1 µg of total RNA using the RevertAid First Strand cDNA Synthesis Kit (Thermo Fisher Scientific) following the manufacturer's instructions and samples were stored at -20ºC until used. qPCR was performed in an Eco® Real-Time PCR System (Illumina, San Diego, CA, USA), using specific primers for AtATG5, AtATG7, and AtACT8 (Table S1), the latter used as a reference gene to normalize gene expression (Graeber et al., 2011; Iglesias-Fernández et al., 2014; Figure S1). For each 10 µl reaction, 2 µl of the samples' cDNA was mixed with 5 µl of FastStart SYBR Green Master (ROX; Hoffmann-La Roche, Basel, Switzerland), 0.25 µl of each primer (final concentration 500 nM), and sterile water up to the final volume. Samples were subjected to thermal-cycling conditions of 95ºC for 10 min, followed by 40 cycles of 10 sec at 95ºC for annealing and 30 sec at 60ºC for extension. The melting curve was designed to increase from 55ºC to 95ºC to calculate the melting temperatures for each PCR product. Amplification of cDNA serial dilutions was performed to estimate primer efficiencies (E), using the formula $E = (10–1/\text{regression line slope} - 1) \times 100$ (Table 1). Expression levels were determined as the number of cycles needed for the amplification to reach a threshold fixed in the exponential phase of the PCR reaction (CT; Pfaffl, 2001).

RNA library construction and RNA-seq analysis

Total RNA was isolated from Col-0 and atg7 seeds as described above. After an additional confirmation of the RNA sample integrity using a Bioanalyzer 2100 (Agilent), the library construction and RNA sequencing (PE150) on Illumina NovaSeq™ 6000 platforms (Illumina, San Diego, CA, USA) were performed by Novogene Genomics Service (Novogene, Beijing, China). For each genotype and treatment, three biological replicates were processed. Library preparation for messenger RNA transcriptome sequencing was purified from total RNA using poly-T oligo-attached magnetic beads. After fragmentation, the first strand cDNA was synthesized using random hexamer

primers, followed by the second strand cDNA synthesis using dTTP for a non-directional library. Samples were subjected to end repair, A-tailing, adapter ligation, size selection, amplification, and purification. Quantification was assessed using Qubit and real-time PCR and the size distribution detection using a bioanalyzer. Quantified libraries were clustered and sequenced on the Illumina platforms and paired-end reads were generated. Raw reads of Fastq format were firstly processed through in-house perl scripts and clean reads were obtained by removing reads containing adapter, ploy-N, and low-quality reads. At the same time, Q20, Q30, and GC content of the clean data were calculated. All the downstream analyses were based on the clean data with high-quality reads mapping to the reference genome, which was downloaded from ensemblplants__A. thaliana_tair10_gca_000001735_1. Hisat2 v2.0.5 was used to build the index of the reference genome and to align paired-end clean reads (Kim et al., 2019; Anders et al., 2015). For differential expression analysis and functional enrichment analysis, the DESeq2 R package was used (1.42.0; Love et al., 2014). The resulting P-values were adjusted using Benjamini and Hochberg's approach for controlling the false discovery rate (FDR; Benjamini and Hochberg, 1995). Genes with an adjusted p-value (padj) ≤ 0.05 found by DESeq2 were assigned as differentially expressed. The data from the 30 samples have been subjected to dimensionality reduction analysis by the FactoExtra package (R software). For GSEA, we used the gseGO function of the clusterProfiler package, the org.At.tair.db for annotation, and the ridge plot function of the ggridges package for visualization (ridgeline plots) (Subramanian et al., 2005). Venn diagrams were made using jvenn tool (Bardou et al., 2014). Heatmaps were constructed using InstantClue v.0.10.10.dev-snap (Nolte et al., 2018) and GO terms' enrichment analysis graphs were generated using ShinyGO 0.77 (Ge et al., 2020).

Fixation, embedding, and sectioning of material for histochemistry

Arabidopsis Col-0, dry and imbibed (24, 48 hoi) seeds were infiltrated with formaldehyde: acetic acid: ethanol: water (3.5:5:50:41.5 by vol.) for 45 min under vacuum (41 mbar) and then incubated at 4ºC for 3 days with gentle shaking as described by Ferrándiz et al. (2000) with modifications. Increasing concentrations of ethanol solutions were used to dehydrate sections and subsequently ethanol was progressively replaced with HistoClear (National Diagnostics, Hessle Hull, England) and then embedded in paraffin. Thin sections of 8 µm were performed with a Leica HistoCore NANOCUT R microtome (Leica) and collected on glass slides. Before histological staining and fluorescent immunolocalization, samples were de-waxed, by repeating the washes in reverse order.

Fluorescent immunolocalization

Seed histological sections were washed with Phosphate Buffered Saline solution (PBS) and digested with 1 mg/ml proteinase-K (Hoffmann-La Roche). Subsequently, slides were incubated at room temperature for 30 min in a blocking solution (Blocking Reagent Roche), and then with primary Anti-APG8A/ATG8A antibody (ab77003; Abcam, Cambridge, UK) at a dilution of 1:1000 in 3% BSA and 0.5% Triton X-100 (Merck) overnight (o/n). After washing with Tris-Buffered Saline (TBS) containing 5 mM Na-Azide, sections were incubated with the secondary Horse Anti-Rabbit IgG Antibody (H+L), DyLight™ 488 (DI-1088-1.5; Thermo Fisher Scientific) for 3h at a dilution of 1:100 in the same buffer. Finally, samples were washed in PBS and water, mounted in CitifluorTM (Sciences Services GmbH, München, Germany), and examined in a confocal microscope (excitation 493 nm, emission 512 nm; Zeiss LSM 880, Jena, Germany).

Polysaccharide and protein histological staining

Seed sections were stained with PAS-NBB: 0.5% (w/v) Periodic Acid (Merck) plus Schiff's reagent (Merck) to detect polysaccharides (pink staining), and with 1% (w/v) Naphthol Blue Black (Merck) to visualize proteins (blue staining). Microscopy analyses were performed on a Zeiss LSM 880 microscope in bright field mode, and the images were captured and processed with the Zen Blue Edition software (Zeiss).

Embryo lipid staining

The coat of Col-0, atg5, and atg7 imbibed seeds (24, 48 hoi) was dissected using hypodermic needles, and embryos were collected in PBS. Then, they were fixed in 4% paraformaldehyde in PBS for 1h under vacuum (41 mbar), washed twice in PBS, and incubated o/n in ClearSee solution (10% xylitol, 15% sodium deoxycholate, 25% urea in distilled water) with gentle agitation. Embryos were stained o/n with 0.05% Nile Red in ClearSee, washed for 30 min and then 1h in ClearSee solution, and mounted in the same solution for imaging on a Zeiss LSM 880 microscope (excitation 561, emission 620 nm) and subsequently processed with Airyscan. Lipid quantification in embryo cells was analyzed using Fiji software and has been expressed as a percentage of lipid area/cell area, in a minimum of 10 distinct embryos per line and germination time.

Yeast two-hybrid (Y2H) assays

For Y2H assays, a mating-based yeast method and the imidazole-glycerol-phosphate dehydratase (HIS3) reporter gene were used. For this, a Saccharomyces cerevisiae J694α (α mating type) library containing a plasmid (pDEST™22, GAL4 activation domain, AD; Thermo Fisher Scientific) collection of 1,200 Open Reading Frames of TFs in A. thaliana was used (Castrillo et al 2011). The yeasts containing the AtABI3 and AtABI5 have been selected for our targeted studies and used as prey. The coding sequence of the AtATG8 gene was amplified from A. thaliana cDNA using primers from Table S1, subcloned into pENTR3C EcoRV and XhoI sites and then cloned into pDEST™32 vector (GAL4 binding domain, BD) by Gateway strategy. This construct was used to transform the S. cerevisiae YM4271a (a mating type) by the polyethylene glycol (PEG) method and utilized as bait. The diploid cells formed after mating were grown onto solid DOB media (Bioworld, Dublin, OH, USA) devoid of leucine and tryptophan. If AtATG8 interacts with AtABI3 and AtABI5 that are fused to BD, the yeast GAL4 TF is reconstituted, and it also becomes Histidine (H) auxotrophic. Increasing concentrations of 3-amino-1,2,4-triazole, an inhibitor of the HIS3 reporter gene (3-AT; Merck), were added to avoid leakage of the HIS3 gene (Castrillo et al., 2011). Positive colonies were visible after 2 to 5 days of incubation at 28ºC.

Western blot

Total protein was extracted from 20 mg Col-0, atg5, and atg7 seeds at different germination time points (0, 36, 48, 72 hoi). For that, dry and germinating seeds were frozen in liquid nitrogen and ground using a Mikro-Dismembrator S (Sartorius AG, Göttingen, Germany). After adding 200 µL of extraction buffer (100 mM Tris-HCl pH 6.8, 4% SDS, 20% glycerol, 200 mM DTT) to the samples, they were vortexed, incubated at 95ºC for 5 min and centrifuged at 18,000 x g for 5 min. Then, supernatants were recovered, and protein was quantified using the Bio-Rad Protein Assay (Bio-Rad, Hercules, CA, USA). Twenty-five µg of protein per well were analyzed in an SDS-PAGE using a Mini-PROTEAN Tetra electrophoresis system (Bio-Rad) and transferred to a Trans-Blot transfer nitrocellulose membrane (Bio-Rad). Membranes were blocked in Tris-buffered saline with 0.1% Tween 20 (TBST; 10mM Tris.HCl, 150 mM NaCl, 0.1% Tween-20, pH 7.5) containing 5% BSA for

1h and probed with a polyclonal anti-ABI5 antibody (1:4,000; Agrisera, Vännäs, Sweden; ref: AS19 4272) o/n at 4ºC. Then, membranes were washed thoroughly with TBST and incubated with a goat anti-rabbit ALP-conjugated antibody (1:10,000; Agrisera; ref: AS09 607) for 1h. Detection was performed using NBT/BCIP stock solution following the manufacturer's instructions (Merck). The intensity signal from the bands was quantified using ImageJ software.

For the western blot analyses in siliques, total protein was extracted from a pool of green siliques taken from entire stems as described in Sánchez-Vicente et al. 2024. Plant tissue was ground using a mortar and pestle and homogenized in 1 volume of extraction buffer (100mM Tris-HCl, 150mM NaCl, 0.25% NP-40) containing 1mM PMSF and 1X cOmplete® EDTA-free protease inhibitor (Sigma), followed by centrifugation for 10 min at 15,800 x g at 4°C. Final protein concentration was quantified as above and Seventy µg of total protein was loaded per well in an SDS-PAGE. Proteins were electrophoretically transferred to an Inmobilon-P polyvinylidene difluoride (PVDF) membrane (Millipore) using the Trans-Blot Turbo (Bio-Rad). Membranes were blocked in Tris buffered saline-0.1% Tween 20 containing 5% blocking agent and probed with antibodies diluted in blocking buffer with 1% blocking agent. Anti-bZIP67 purified rabbit immunoglobulin (Biomedal, 1:100), anti-Actin (Sigma-Merck, 1: 10,000), ECL-Peroxidase-labelled anti-rabbit (Amersham, 1:10,000) and anti-mouse (Amersham, 1:10,000) antibodies were used in the western blot analyses. Detection was performed using ECL Advance Western Blotting Detection Kit (Amersham) and the chemiluminescence was detected using an ChemiDoc Imaging System (BioRad).

REFERENCES

Abraham, Z., Iglesias-Fernández, R., Martínez, M., Rubio-Somoza, I., Díaz, I., Carbonero, P., Vicente-Carbajosa, J. (2016). A developmental switch of gene expression in the barley seed mediated by HvVP1 (Viviparous-1) and HvGAMYB Interactions. *Plant Physiology,* **170**, 2146-2158.

Albertos, P., Romero-Puertas, M.C., Tatematsu, K., Mateos, I., Sánchez-Vicente, I., Nambara, E., Lorenzo, O. (2015). S-nitrosylation triggers ABI5 degradation to promote seed germination and seedling growth. *Nature Communications,* **6,** 8669.

Ali, F., Qanmber, G., Li, F., Wang, Z. (2021). Updated role of ABA in seed maturation, dormancy, and germination. *Journal of Advanced Research,* **35**, 199-214.

Anders, S., Pyl, P.T., Huber, W. (2015). HTSeq—a Python framework to work with high-throughput sequencing data. *Bioinformatics* **31**, 166-169.

Avin-Wittenberg, T., Bajdzienko, K., Wittenberg, G., Alseekh, S., Tohge, T., Bock, R., Giavalisco, P., Fernie, A.R. (2015). Global analysis of the role of autophagy in cellular metabolism and energy homeostasis in Arabidopsis seedlings under carbon starvation. Plant Cell. 27, 306-22.

Bardou, P., Mariette, J., Escudié, F., Djemiel, C., Klopp, C. (2014). jvenn: an interactive Venn diagram viewer. BMC Bioinformatics, 15, 293.

Barros, J.A.S., Cavalcanti, J.H.F., Medeiros, D.B., Nunes-Nesi, A., Avin-Wittenberg, T., Fernie, A.R., Araújo, W.L. (2017). Autophagy deficiency compromises alternative pathways of respiration following energy deprivation in Arabidopsis thaliana. Plant Physiology, 175, 62-76.

Baud, S., Dubreucq, B., Miquel, M., Rochat, C., Lepiniec, L. (2008). Storage reserve accumulation in Arabidopsis: metabolic and developmental control of seed filling. In Arabidopsis Book. 6:e0113.

Bedu, M., Marmagne, A., Masclaux-Daubresse, C., Chardon, F. (2020). Transcriptional plasticity of autophagy-related genes correlates with the genetic response to nitrate starvation in Arabidopsis thaliana. Cells, 9, 1021.

Benjamini, Y., Hochberg, Y. (1995). Controlling the False Discovery Rate: a practical and powerful approach to multiple testing. Journal of the Royal Statistical Society, Series B (Methodology), 57, 289-300.

Bentsink, L., Jowett, J., Hanhart, C.J., Koornneef, M. (2006). Cloning of DOG1, a quantitative trait locus controlling seed dormancy in Arabidopsis. Proceedings of the National Academy of Sciences of the United States of America, 103, 17042-17047.

Bewley, J.D., Bradford, K.J., Hilhorst, H.W.M., Nonogaki, H. (2013) Structure and composition. In Seeds, Bewley, J.D., Bradford, K.J., Eds.; Springer: New York, NY, USA, 2013; pp. 85–131.

Carbonero, P., Iglesias-Fernández, R., Vicente-Carbajosa, J. (2017). The AFL subfamily of B3 transcription factors: evolution and function in angiosperm seeds. Journal of Experimental Botany, 68, 871-880.

Carrillo-Barral, N., Rodríguez-Gacio, M.D.C., Matilla, A.J. (2020). Delay of Germination-1 (DOG1): a key to understanding seed dormancy. Plants (Basel). 9, 480.

Castrillo, G., Turck, F., Leveugle, M., Lecharny, A., Carbonero, P., Coupland, G., Paz-Ares, J., Oñate-Sánchez, L. (2011). Speeding cis-trans regulation discovery by phylogenomic analyses coupled with screenings of an arrayed library of Arabidopsis transcription factors. PloS ONE 6, e21524.

Chen, K., Yin, Y., Liu, S., Guo, Z., Zhang, K., Liang, Y., Zhang, L., Zhao, W., Chao, H., Li, M. (2019). Genome-wide identification and functional analysis of oleosin genes in Brassica napus L. BMC Plant Biology, 19, 294.

Chen, L. Lv, Q, Yang, W, Yang, H, Chen, Q, Wang, B, Lei, Y., Xie, Y. (2022). TaNBR1, a novel wheat NBR1-like domain gene negatively regulates drought stress tolerance in transgenic Arabidopsis. International Journal of Molecular Sciences, 23, 4519.

Clough, S.J., Bent, A.F. (1998). Floral dip: a simplified method for Agrobacterium-mediated transformation of Arabidopsis thaliana. The Plant Journal, 16, 735–743.

Di Berardino, J., Marmagne, A., Berger, A., Yoshimoto, K., Cueff, G., Chardon, F., Masclaux-Daubresse, C., Reisdorf-Cren, M. (2018). Autophagy controls resource allocation and protein storage accumulation in Arabidopsis seeds. Journal of Experimental Botany, 69, 1403–1414.

Ding, X., Zhang, X., Otegui, M.S. (2018). Plant autophagy: new flavors on the menu. Current Opinion in Plant Biology, 46, 113–121.

Dobrenel, T., Caldana, C., Hanson, J., Robaglia, C., Vincentz, M., Veit, B., Meyer C. (2016). TOR signaling and nutrient sensing. Annual Review of Plant Biology, 67, 261-85.

Ellgaard, L., Helenius, A. (2003). Quality control in the endoplasmic reticulum. Nature Reviews Molecular Cell Biology, 4, 181–191.

Erlichman, O.A., Weiss, S., Arkia, M.A., Ankary-Khaner, M., Soroka, Y., Jasinska, W., Rosental, L., Brotman, Y., Avin-Wittenberg, T. (2023). Autophagy in maternal tissues contributes to Arabidopsis seed development. Plant Physiology, 193, 611-626.

Fan, J., Yu, L., Xu, C. (2019). Dual role for autophagy in lipid metabolism in Arabidopsis. The Plant Cell, 31, 1598–1613.

Ferrándiz, C., Liljegren, S.J., Yanofsky, M.F. (2000). Negative regulation of the SHATTERPROOF genes by FRUITFULL during Arabidopsis fruit development. Science, 289, 436-8.

Finch-Savage, W.E., Bassel, G.W. (2016). Seed vigour and crop establishment: extending performance beyond adaptation. Journal of Experimental Botany, 67, 567–591.

Finkelstein, R.R. (1994). Mutations at two new Arabidopsis ABA response loci are similar to the abi3 mutations. The Plant Journal, 5, 765-771.

Fraiberg M, Elazar Z. (2020). Genetic defects of autophagy linked to disease. Progress in Molecular Biology and Translational Science, 172, 293-323.

Ge, S.X., Jung, D., Yao, R. (2020) ShinyGO: a graphical gene-set enrichment tool for animals and plants. Bioinformatics, 36, 2628-2629.

Graeber, K., Linkies, A., Wood, A.T.A., Leubner-Metzger, G.A. (2011). Guideline to family-wide comparative state-of-the-art quantitative RT-PCR analysis exemplified with a Brassicaceae cross-species seed germination case study. The Plant Cell, 23, 2045-2063.

Guiboileau, A., Avila-Ospina, L., Yoshimoto, K., Soulay, F., Azzopardi, M., Marmagne, A., Lothier, J., Masclaux-Daubresse, C. (2013). Physiological and metabolic consequences of autophagy deficiency for the management of nitrogen and protein resources in Arabidopsis leaves depending on nitrate availability. New Phytologist, 199, 683–694.

Guiboileau, A., Yoshimoto, K., Soulay, F., Bataillé, M., Avice, J.C., Masclaux-Daubresse, C. (2012) Autophagy machinery controls nitrogen remobilization at the whole-plant level under both limiting and ample nitrate conditions in Arabidopsis. New Phytologist, 194, 732–740.

Havé, M., Luo, J., Tellier, F., Balliau, T., Cueff, G., Chardon, F., Zivy, M., Rajjou, L., Cacas, J.L., Masclaux-Daubresse, C. (2019). Proteomic and lipidomic analyses of the Arabidopsis atg5 autophagy mutant reveal major changes in endoplasmic reticulum and peroxisome metabolisms and in lipid composition. New Phytologist, 223, 1461-1477.

Hills, M.J. (2004). Control of storage-product synthesis in seeds. Current Opinion in Plant Biology, 7, 302-308.

Hofius, D., Schultz-Larsen, T., Joensen, J., Tsitsigiannis, D.I., Petersen, N.H.T., Mattsson, O., Jørgensen, L.B., Jones, J.D.G., Mundy, J., Petersen, M. (2009). Autophagic components contribute to hypersensitive cell death in Arabidopsis. Cell, 137, 773-783.

Holdsworth, M.J., Bentsink, L., Soppe, W.J.J. (2008). Molecular networks regulating Arabidopsis seed maturation, after-ripening, dormancy and germination. New Phytologist, 179, 33-54.

Iglesias-Fernández, R., Vicente-Carbajosa, J. (2022). A view into seed autophagy: from development to environmental responses. Plants, 11, 3247.

Iglesias-Fernández, R., Wozny, D., Iriondo-de Hond, M., Oñate-Sánchez, L., Carbonero, P., Barrero-Sicilia, C. (2014). The AtCathB3 gene, encoding a cathepsin B-like protease, is expressed during germination of Arabidopsis thaliana and transcriptionally repressed by the basic leucine zipper protein GBF1. Journal of Experimental Botany, 65, 2009–2021.

Jefferson, R.A., Kavanagh, T.A., Bevan, M.W. (1987). GUS fusions: beta-glucuronidase as a sensitive and versatile gene fusion marker in higher plants. The EMBO Journal 6, 3901-3907.

Joosen, R.V.L., Kodde, J., Willems, L.A.J., Ligterink, W., Van Der Plas, L.H.V., Hilhorst, H.W.M. (2010). Germinator: a software package for high-throughput scoring and curve fitting of Arabidopsis seed germination. The Plant Journal, 62, 148-159.

Jurkiewicz, P., Melser, S., Maucourt, M., Ayeb, H., Veljanovski, V., Maneta-Peyret, L., Hooks, M., Rolin, D., Moreau, P., Batoko, H. (2018). The multistress-induced Translocator protein (TSPO) differentially modulates storage lipids metabolism in seeds and seedlings. The Plant Journal, 96, 274-286.

Kellner, R., De la Concepcion, J.C., Maqbool, A., Kamoun, S., Dagdas, Y.F. (2017). ATG8 expansion: A driver of selective autophagy diversification? Trends in Plant Science, 22, 204–214.
Kim, D., Paggi, J.M., Park, C., Bennett, C., Salzberg, S.L. (2019). Graph-based genome alignment and genotyping with HISAT2 and HISAT-genotype. Nature Biotechnology, 37, 907-915.

Kim, Y.Y., Jung, K.W., Yoo, K.S., Jeung, J.U., Shin, J.S. (2011). A stress-responsive caleosin-like protein, AtCLO4, acts as a negative regulator of ABA responses in Arabidopsis. Plant and Cell Physiology, 52, 874-884.

Koornneef, M., Reuling, G., Karssen, C. M. (1984). The isolation and characterization of abscisic acid-insensitive mutants of Arabidopsis thaliana. Physiologia Plantarum, 61, 377-383.

Li, F., Chung, T., Pennington, J.G., Federico, M.L., Kaeppler, H.F., Kaeppler, S.M., Otegui, M.S., Vierstra, R.D. (2015). Autophagic recycling plays a central role in maize nitrogen remobilization. The Plant Cell 27, 1389–1408.

Liu, Y., Xiong, Y., Bassham, D.C. (2009). Autophagy is required for tolerance of drought and salt stress in plants. Autophagy, 5, 954-963.

Liu, Z., Yang, Q., Wu, P., Li, Y., Lin, Y., Liu, W., Guo, S., Liu, Y., Huang, Y., Xu, P., Qian, Y., Xie, Q. (2023). Dynamic monitoring of TGW6 by selective autophagy during grain development in rice. New Phytologist 240, 2419-2435.

López-Molina, L., Mongrand, S., Chua, N.H. (2001). A postgermination developmental arrest checkpoint is mediated by abscisic acid and requires the ABI5 transcription factor in Arabidopsis. Proceedings of the National Academy of Sciences of the United States of America 98, 4782-4787.

Love, M.I., Huber, W. and Anders, S. (2014). Moderated estimation of fold change and dispersion for RNA-seq data with DESeq2. Genome Biology, 15, 550.

Luo, S., Li, X., Zhang, Y., Fu, Y., Fan, B., Zhu, C., Chen, Z. (2021) Cargo recognition and function of selective autophagy receptors in plants. International Journal of Molecular Sciences, 22, 1013.

Marshall, R.S., Hua, Z., Mali, S., McLoughlin, F., Vierstra, R.D. (2019). ATG8-binding UIM proteins define a new class of autophagy adaptors and receptors. Cell, 177, 766-781.e24.

Masclaux-Daubresse, C., Clément, G., Anne, P., Routaboul, J.M., Guiboileau, A., Soulay, F., Shirasu, K., Yoshimoto, K. (2014). Stitching together the multiple dimensions of autophagy using metabolomics and transcriptomics reveals impacts on metabolism, development, and plant responses to the environment in Arabidopsis. The Plant Cell, 26, 1857–1877.

Matilla, A.J. (2022). Exploring breakthroughs in three traits belonging to seed life. Plants, 11, 490.

Maurel, C., Boursiac, Y., Luu, D.T., Santoni, V., Shahzad, Z., Verdoucq, L. (2015). Aquaporins in Plants. Physiological Reviews,, 1321-1358.

Mendes, A.T., Kelly, A.A., Erp, H.V., Shaw, E., Powers, S.J., Kurup, S., Eastmondb, P.J. (2013). bZIP 67 regulates the omega-3 fatty acid content of Arabidopsis seed oil by activating FATTY ACID DESATURASE 3. The Plant Cell, 25, 3104–3116.

Michaeli, S., Galili, G., Genschik, P., Fernie, A.R., Avin-Wittenberg, T. (2016). Autophagy in plants-what's new on the menu? Trends in Plant Science, 21, 134-144.

Michalak, K.M., Wojciechowska, N., Marzec-Schmidt, K., Bagniewska-Zadworna, A. (2024). Conserved autophagy and diverse cell wall composition: Unifying features of vascular tissues in evolutionarily distinct plants. Annals of Botany, mcae015.

Miklaszewska, M., Zienkiewicz, K., Klugier-Borowska, E., Rygielski, M., Feussner, I., Zienkiewicz, A. (2023). CALEOSIN 1 interaction with AUTOPHAGY-RELATED PROTEIN 8 facilitates lipid droplet microautophagy in seedlings. Plant Physiology, 193, 2361-2380.

Minina, E.A., Moschou, P.N., Vetukuri, R.R., Sanchez-Vera, V., Cardoso, C., Liu, Q., Elander, P.H., Dalman, K., Beganovic, M., Yilmaz, J.L., Marmon, S., Shabala, L., Suarez, M.F., Ljung, K., Novák, O., Shabala, S., Stymne, S., Hofius, D., Bozhkov, P.V. (2018). Transcriptional stimulation of rate-limiting components of the autophagic pathway improves plant fitness. Journal of Experimental Botany, 69, 1415-1432.

Müntz, K. (2007). Protein dynamics and proteolysis in plant vacuoles. Journal of Experimental Botany, 58, 2391–2407.

Naested, H., Frandsen, G.I., Jauh, G.Y., Hernandez-Pinzon, I., Nielsen, H.B., Murphy, D.J., Rogers, J.C., Mundy, J. (2000). Caleosins: Ca2+-binding proteins associated with lipid bodies. Plant Molecular Biology, 44, 463-476.

Nakabayashi, K., Okamoto, M., Koshiba, T., Kamiya, Y., Nambara, E. (2005). Genome-wide profiling of stored mRNA in Arabidopsis thaliana seed germination: Epigenetic and genetic regulation of transcription in seed. The Plant Journal, 41, 697–709.

Nolte, H., MacVicar, T.D., Tellkamp, F., Krüger, M. (2018). Instant Clue: a software suite for interactive data visualization and analysis. Scientific Reports, 8, 12648.

Ohlsson, J.A., Leong, J.X., Elander, P.H., Ballhaus, F., Holla, S., Dauphinee, A.N., Johansson, J., Lommel, M., Hofmann, G., Betnér, S., Sandgren, M., Schumacher, K., Bozhkov, P.V., Minina, E.A. (2023). SPIRO - the automated Petri plate imaging platform designed by biologists, for biologists. The Plant Journal, doi: 10.1111/tpj.16587.

Okamoto, T., Shimada, T., Hara-Nishimura, I., Nishimura, M., Minamikawa, T. (2003). C-terminal KDEL sequence of a KDEL-tailed cysteine proteinase (sulfhydryl-endopeptidase) is involved in formation of KDEL vesicle and in efficient vacuolar transport of sulfhydryl-endopeptidase. Plant Physiology, 132, 1892–1900.

Oñate-Sánchez, L., Vicente-Carbajosa, J. (2008). DNA-free RNA isolation protocols for Arabidopsis thaliana, including seeds and siliques. BMC Research Notes, 1, 93.

Pfaffl, M.W. (2001). A new mathematical model for relative quantification in quantitative RT-PCR. Nucleic Acids Research, 29, e45.

Poxleitner, M., Rogers, S.W., Lacey Samuels, A., Browse, J., Rogers, J.C. (2006). A role for caleosin in degradation of oil-body storage lipid during seed germination. The Plant Journal, 47, 917-933.

Qi, H., Xia, F.N., Xiao, S. (2021). Autophagy in plants: Physiological roles and post-translational regulation. Journal of Integrative Plant Biology, 63, 161–179.

Qin, Z., Wang, T., Zhao, Y., Ma, C., Shao, Q. (2023). Molecular machinery of lipid droplet degradation and turnover in plants. International Journal of Molecular Sciences, 24, 16039.

Reeves, W.M., Lynch, T.J., Mobin, R., Finkelstein, R.R. (2011). Direct targets of the transcription factors ABA-Insensitive(ABI)4 and ABI5 reveal synergistic action by ABI4 and several bZIP ABA response factors. Plant Molecular Biology, 75, 347-63.

Sajeev, N., Koornneef, M., Bentsink, L. (2024). A commitment for life: Decades of unraveling the molecular mechanisms behind seed dormancy and germination. The Plant Cell. 12, koad328.

Sánchez-Vicente, I., Albertos, P., Mata-Pérez, C., Barroso, J.B., Lorenzo O. (2024). Reversible S-nitrosylation of bZIP67 by peroxiredoxin IIE activity and nitro-fatty acids determines the plant lipid profile. Cell Reports, In. press.

Sawa-Makarska, J., Baumann, V., Coudevylle, N., von Bülow S., Nogellova, V., Abert, C., Schuschnig, M., Graef, M., Hummer, G., Martens S. (2020). Reconstitution of autophagosome nucleation defines Atg9 vesicles as seeds for membrane formation. Science, 369, eaaz7714.

Sera, Y., Hanamata, S., Sakamoto, S., Ono, S., Kaneko, K., Mitsui, Y., Koyano, T., Fujita, N., Sasou, A., Masumura, T., Saji, H., Nonomura, K.I., Mitsuda, M., Mitsui, T., Kurusu, T., Kuchitsu, K. (2019). Essential roles of autophagy in metabolic regulation in endosperm development during rice seed maturation. Scientific Reports, 9, 18544.

Shao, Q., Liu, X., Su, T., Ma, C., Wang, P. (2019). New insights into the role of seed oil body proteins in metabolism and plant development. Frontiers in Plant Science, 10, 1568.

Siénko, K., Poormassalehgoo, A., Yamada, K., Goto-Yamada, S. (2020). Microautophagy in plants: consideration of its molecular mechanism. Cells, 9, 887.

Siloto, R.M., Findlay, K., Lopez-Villalobos, A., Yeung, E.C., Nykiforuk, C.L., Moloney, M.M. (2006). The accumulation of oleosins determines the size of seed oilbodies in Arabidopsis. The Plant Cell, 18, 1961-74.

Stephani, M., Picchianti, L., Gajic, A., Beveridge, R., Skarwan, E., Sanchez de Medina Hernandez, V., Mohseni, A., Clavel, M., Zeng, Y., Naumann, C., Matuszkiewicz, M., Turco, E., Loefke, C., Li, B., Dürnberger, G., Schutzbier, M., Chen, H.T., Abdrakhmanov, A., Savova, A., Chia, K.S., Djamei, A., Schaffner, I., Abel, S., Jiang, L., Mechtler, K., Ikeda, F., Martens, S., Clausen, T., Dagdas, Y. (2020). A cross-kingdom conserved ER-phagy receptor maintains endoplasmic reticulum homeostasis during stress. eLife, 9, e58396.

Su, T., Li, X., Yang, M., Shao, Q., Zhao, Y., Ma, C., Wang, P. (2020). Autophagy: An intracellular degradation pathway regulating plant survival and stress response. Frontiers in Plant Science, 11, 164.

Subramanian, A., Tamayo, P., Mootha, V.K., Mukherjee, S., Ebert, B.L., Gillette, M.A., Paulovich, A., Pomeroy, S.L., Golub, T.R., Lander, E.S., Mesirov, J.P. (2005). Gene set enrichment analysis: a knowledge-based approach for interpreting genome-wide expression profiles. Proceedings of the National Academy of Sciences of the United States of America, 102, 15545-1550.

Tarnowski, L., Rodriguez, M.C., Brzywczy, J., Piecho-Kabacik, M., Krcˇkova, Z., Martinec, J., Wawrzynska, A., Sirko, A. (2020). A selective autophagy cargo receptor NBR1 modulates abscisic acid signalling in Arabidopsis thaliana. Scientific Reports, 10, 7778.

Thompson, A.R., Doelling, J.H., Suttangkakul, A., Vierstra, R.D. (2005). Autophagic nutrient recycling in Arabidopsis directed by the ATG8 and ATG12 conjugation pathways. Plant Physiology 138, 2097-110.

Tian, R., Wang, F., Zheng, Q., Niza, V.M.A.G.E., Downie, A.B., Perry, S.E. (2020). Direct and indirect targets of the arabidopsis seed transcription factor ABSCISIC ACID INSENSITIVE3. The Plant Journal, 103, 1679-1694.

Vitale, A., Pedrazzini, E. (2022). StresSeed: The unfolded protein response during seed development. Frontiers in Plant Science, 13, 869008.

Wesch, N, Kirkin, V., Rogov, V.V. (2020). Atg8-family proteins-structural features and molecular interactions in autophagy and beyond. Cells. 9, 2008.

Xie, Z., Klionsky, D. J. (2007). Autophagosome formation: core machinery and adaptations. Nature Cell Biology, 9, 1102–1109.

Yan, H., Zhuang, M., Xu, X., Li, S., Yang, M., Li, N., Du, X., Hu, K., Peng, X., Huang, W., Wu, H., Tse, Y.C., Zhao, L., Wang, H. (2023). Autophagy and its mediated mitochondrial quality control maintain pollen tube growth and male fertility in Arabidopsis. Autophagy, 19, 768-783.

Yang, M., Wang, L., Chen, C., Guo, X., Lin, C., Huang, W., Chen, L. (2021). Genome-wide analysis of autophagy-related genes in Medicago truncatula highlights their roles in seed development and response to drought stress. Scientific Reports, 11, 22933.

Yang, X., Srivastava, R., Howell, S.H., Bassham, D.C. (2016). Activation of autophagy by unfolded proteins during endoplasmic reticulum stress. The Plant Journal, 85, 83–95.

Yang, Z., Klionsky, D.J. (2010). Mammalian autophagy: core molecular machinery and signaling regulation. Current Opinion in Plant Biology, 22, 124-31.

Yoshimoto, K., Jikumaru, Y., Kamiya, Y., Kusano, M., Consonni, C., Panstruga, R., Ohsumi, Y., Shirasu, K. (2009). Autophagy negatively regulates cell death by controlling NPR1-dependent salicylic acid signaling during senescence and the innate immune response in Arabidopsis. The Plant Cell, 21, 2914–2927.

Yu, P., Hua, Z. (2022). The ubiquitin-26S proteasome system and autophagy relay proteome homeostasis regulation during silique development. The Plant Journal, 111, 1324-1339.

Yuan, Y., Cao, X., Zhang, H., Liu, C., Zhang, Y., Song, X.L., Gai, S. (2021). Genome-wide identification and analysis of Oleosin gene family in four cotton species and its involvement in oil accumulation and germination. BMC Plant Biology, 21, 569.

Zhao, Y., Dong, Q., Geng, Y., Ma, C., Shao, Q. (2023). Dynamic regulation of lipid droplet biogenesis in plant cells and proteins involved in the process. International Journal of Molecular Sciences, 24, 7476.

Zhuang, X., Li, B., Jiang, L. (2024). Autophagosome biogenesis and organelle homeostasis in plant cells. The Plant Cell, koae099.

ACKNOWLEDGMENTS

This work was supported by projects BIO2017-82873-R (J.V.C and R.I-F.), Quinoa4Med (PRIMA-AEI, ref: PCI2022-132988; R.I.F.), and PID2020-119731RB-I00, funded by MCIN/AEI/10.13039/501100011033 (MCIN/AEI), and projects SA137P20 and SA142P23 from the Regional Government of Castile and Leon and "Escalera de Excelencia" CLU-2018-04 co-funded by the FEDER Operative Program of Castile and Leon 2014–2020 Spain (to O.L.).

The authors kindly thank Prof. A. Matilla for the critical reading of the manuscript.

LEGENDS TO FIGURES

Figure 1. Temporal and spatial expression of *AtATG5* and *AtATG7* genes in adult plants. (a) Expression data of *AtATG5* and *AtATG7* were obtained from the Gene Expression Tool at the Bio-Analytic Resource for Plant Biology (BAR) public database and represented as a heatmap (scale 0-500 GCOS units). GUS histochemical staining of different organs and tissues from *PAtATG5::uidA* (b) and *PAtATG7: uidA* (c) transgenic adult plants.

Figure 2. Expression patterns of *AtATG5* and *AtATG7* genes during embryogenesis, seed maturation and germination. (a) Images display the developmental stages of siliques used in the qPCR assays, along with corresponding patterns of silique weight, cell expansion, cell division, and ABA accumulation during silique development. Transcript analysis of *AtATG5* and *AtATG7* during seed embryogenesis and maturation is shown in (b), while (c) illustrates their expression during imbibition. (d) GUS histochemical staining of different *PAtATG5::uidA* and *PAtATG7::uidA* embryos at different time points (hours) of imbibition (hoi). Early Green stages 1 and 2 (EG1 and EG2), Late Green stages 1 and 2 (LG1 and LG2), and Brown (B) seeds. Data is shown as means ± standard error (SE) of three independent experiments, normalized to the expression of the *AtACT-7* gene.

Figure 3. Germination assays in *atg5, atg7, abi5-7* mutant lines, and Col-0 (control) in the presence and absence of 1 µM ABA. Means ± SE of three independent replicates are represented. SCR: Seed Coat Rupture; ER: Endosperm Rupture, *sensu stricto* germination. In the inset, the time required to achieve 50% seed coat rupture (t_{50} SCR) and endosperm rupture (t_{50} ER) is indicated.

Figure 4. Differentially expressed genes (DEG) analysis in *atg7* in comparison to Col-0 at 24 hoi. (a) The volcano plot displays DEG as red dots, meeting the criteria of *p*-adj. ≤ 0.05 and Log_2FC ≤ 2. Some of the most significant DEGs such as *AtCLO1, CRC, ATPDI10, AtCRT1b, SEIPIN1, and ALPHA-TIP* are highlighted in boxes. (b) GSEA categorizes all DEG into different GOs represented as curves ranked according to their Log_2FC. The categories highlighted in red are further analyzed. (c) The heatmaps show the expression of the DEG meeting the criteria in (a) included in selected GO categories from (b). Additional DEG not included in the selected categories from (b) are shown in the heatmap on the right. NS, non-significant; Log_2FC, Log_2 fold change; *p*-adj, *p*-adjusted.

Figure 5. Differences in lipid content in *A. thaliana* Col-0, *atg5*, and *atg7* embryos at 24 and 48 hoi. (a) Differential Interference Contrast (DIC) images at x10 magnification show the entire embryos, with the radicle area used for lipid visualization and lipid content analysis marked with a rectangle. Confocal images of Nile Red lipid staining of individual embryo cells are visualized at x60 magnification. (b) Lipid content analysis of individual cells represented as % lipid area/cell area in the different *A. thaliana* lines. Data shown are means± SE of at least 10 independent cells. Letters indicate statistically significant differences among the three Arabidopsis lines (p≤0.05, One-way ANOVA followed by Turkey's comparisons test).

Figure 6. Differences in protein organization in *A. thaliana* Col-0, *atg5*, and *atg7* dry (0 hoi) and 24 and 48 hoi seed sections. Periodic acid (PAS)- Naphthol Blue Black (NBB) staining of protein and polysaccharides is shown for Col-0 (a-f), *atg5* (g-l), and *atg7* (m-r) seed transversal sections.

Images of DS (a, g, m), at 24 hoi (c, i, o) and at 48 hoi (e, k, q) taken at 25x magnification, showing with a white rectangle indicating the close-up image taken at 60x magnification for DS (b, h, n), at 24 hoi (d, j, p) and 48 hoi (f, l, r). R, radicle; C, cotyledon; PSV, Protein Storage Vacuoles; SG, starch grain.

Figure 7. Differences in PSV organization in *A. thaliana* Col-0, *atg5*, and *atg7* germinating seed sections. Confocal images showing AtATG8 immunolocalization in Col-0 (a-c), *atg5* (e-g), and *atg7* (i-k) seed transversal sections at 40x magnification (a, e, i), 63x magnification (b, f, j) and a close-up image from x63 magnification, indicated with a white rectangle (c, g, k). DIC images at x40 magnification are also shown (d, h, l). R, radicle; C, cotyledon; PSV, Protein Storage Vacuoles.

Figure 8. Transcriptomic analysis of the specific ABA response in *atg7* and Col-0 imbibed seeds. (a) The Venn diagram shows specific and shared induced or repressed genes due to the effect of ABA in each line, in similar seed physiological stages (96 hoi in the presence of ABA and 48 hoi in the absence; upper panel). A significant number of genes show ABA-specific induction in *atg7* and repression in Col-0 and vice-versa and are marked in a circle. A bar diagram depicts the number of genes that are induced or repressed in each sample (bottom panel). (b) The heatmap displays the expression data of the DEG marked in a circle in (a) and the GO enrichment analysis of these DEGs. (c) The heatmap illustrates the expression data of the DEG that show ABA-specific repression in Col-0 and induction in *atg7*, at different seed maturation stages, retrieved from the Bio-Analytic Resource for Plant Biology (BAR) database. Genes in red letters are included in the response to the ABA pathway in the GO enrichment analysis, while genes in green are included in other categories. Genes encoding proteins that are putative targets for AtABI3 and AtABI5 are indicated (data taken from Reeves *et al*., 2011, and the genes marked with asterisks (*) obtained from Tian *et al*., 2020). DS, dry seed; hoi, hours of imbibition.

Figure 9. AtATG8H specifically binds to AtABI3 and AtABI5 proteins in a Y2H experiment and AtABI5 degradation is delayed in *atg5* and *atg7* mutants. (a) Growth of yeast diploid cells expressing the GAL4 binding domain fused to ATG8H (BD-ATG8H) and the GAL4 activation domain fused to ABI3 or ABI5 (AD-ABI3 or AD-ABI5) in selective medium (–L, –W, –H) with increasing concentrations of 3-AT. The lack of growth of the negative controls BD-⌀ and AD-⌀ is also displayed. (b) Western blot analysis of AtABI5 in *A. thaliana* Col-0, *atg5* and *atg7* dry (0 hoi) and germinating seeds (36, 48, 72 hoi). (c) The ABI5 band intensity from western blot analysis in (b) is calculated by densitometry.

Figure 10. Proposed model of the integrative role of autophagy in early seed imbibition. According to our data, under non-stress conditions, autophagy is crucial in controlling lipid turnover and protein storage mobilisation during germination. The ABA signal transduction pathway leads to modifications of downstream targets like ABI3 and ABI5, modulating their activity and participation in the accumulation / mobilisation of storage compounds and responses to environmental signals. The degradation of these transcription factors is critical for seed germination, and the contribution of autophagy represents a balance between normal growth and amplifying ABA signaling input in response to adaptation to the environment.

LEGENDS TO SUPPORTING FIGURES, TABLES AND DATA

Figure S1. Expression profile of the genes included in Autophagy GO term (GO:0006914; Biological Process) at different seed developmental stages, represented as a heatmap. Gene expression is retrieved from the Gene Expression Tool at the Bio-Analytic Resource for Plant Biology (BAR) public database (https://bar.utoronto.ca/) and is expressed as the average log_2FC of three replicates, in comparison to their controls by using Heatmapper tool. Gene set includes not only ATG, but also those genes encoding VPS, autophagy receptors (e.g., NBR1), TFs (e.g., WRKY33), and factors involved in endoplasmic reticulum stress perception (e.g., IRE1). Expression remains relatively constant across diverse samples, including various silique stages (3-10), DS, and seeds imbibed for 1, 3, 6, 12 and 24 hoi. The *TIP3;1* gene (*At1g73190*; alpha-tonoplast intrinsic protein) stands out for its high expression across all silique stages and dry seed. Gene copy number data taken from the Plaza tool (https://bioinformatics.psb.ugent.be/plaza) are also included. DS, dry seed; hoi, hours of imbibition.

Figure S2. Expression profile of *AtACT-7* reference gene. Samples are from Col-0, *atg5*, *atg7*, and *abi5-7* germinating seeds, from Col-0 siliques at different seed maturation stages, and Col-0 seeds at different time points (hours) of imbibition (hoi). Early Green seeds stages 1 and 2 (EG1 and EG2), Late Green seeds stages 1 and 2 (LG1 and LG2), and Brown seeds (B). Data are presented as means ±SE of two technical replicates of three biological samples.

Figure S3. Expression of *AtATG5, AtATG7* and *AtABI5* genes in Col-0, *atg5*, *atg7* and *abi5-7* DS. Relative expression is referred to *AtACT-7* gene expression.

Figure S4. Expression of *AtATG5* and *AtATG7* genes during embryogenesis in the absence (control) and the presence of ABA. (a) GUS histochemical staining of PAtATG5::uidA and PAtATG7::uidA embryos at 24 and 48 hoi in the absence or presence of 1 µM ABA. (b) Transcription analysis by qPCR at 36 hoi in the absence or presence of 0.5 µM ABA. Data are presented as means ± SE from three independent experiments and normalized to the expression of the *AtACT-7* gene.

Figure S5. RNAseq experiment design and quality analysis. (a) Design of the RNAseq experiment. Col-0 and *atg7* DS, as well as imbibed seeds in the absence (24, 48 hoi) and in the presence of ABA (96 hoi), were collected for RNAseq analysis in triplicate. The germination status of the seeds when collected (non-germinated or a mixture of germinated + non-germinated) are drawn. (b) Heatmap showing the expression data of DEG meeting the criteria p-adj $\leq$ 0.05 and $Log_2FC \leq 2$. The colored bar on the top indicates Col-0 samples in blue and *atg7* samples in coral. Abbreviations of the samples' name: D, dry seed; A, in presence of ABA; 24, 24 hoi; 48, 48 hoi; 96, 96 hoi; _1, replicate 1; _2, replicate 2; _3, replicate 3. (c) Two-dimensional PCA of the RNAseq samples. (d) Scree plot of RNAseq samples, showing the percentage of explained variances in each dimension.

Figure S6. Negative controls of Nile Red lipid staining were performed on *A. thaliana* Col-0, *atg5*, and *atg7* unstained embryos at 24 and 48 hoi. DIC images of the entire embryos were captured at x10 magnification and confocal images were taken at 60x magnification under the same conditions as in Figure 6.

Figure S7. Negative controls of AtATG8 immunolocalization performed on germinating seed sections of *A. thaliana* Col-0. Confocal images taken at 40x magnification (a, d, g), at 60x magnification (b, e, h), and DIC images at 40x magnification (c, f, i) of the control samples incubated with primary antibody but not secondary (a-c), secondary antibody but not primary (d-f) and without any antibody (g, h, i). Images were taken in the same conditions as in Figure 7. R, radicle; C, cotyledon.

Figure S8. ATG8 Interacting Motifs (AIMs) found in AtABI3 and AtABI5. The consensus sequence of AIMs is considered as Θ-X-X-Γ, where Θ is an aromatic (W/F/Y) and Γ is a hydrophobic (L/I/V) residue (Wesch *et al*., 2020).

Figure S9. AtbZIP67 and its target genes accumulation in AtATG mutant lines. (a) Western blot analysis of AtbZIP67 in *A. thaliana* siliques from Col-0, *atg5*, *atg7* and the overexpression lines oeATG5 and oeATG7 at different temperatures (15ºC and 23ºC). (b) AIMs found in the *AtbZIP67* gene sequence. (c) Expression of AtbZIP67 target genes in the RNAseq analysis comparing the effect of the presence of ABA in *atg7* and Col-0 lines (96 hoi in the presence of ABA vs 48 hoi in the absence).

Table S1. Sequences of primers used in this work.

Data S1. List of genes found in the AmiGO server using autophagy Gene Ontology term and their expression in siliques and seeds retrieved from the Gene Expression Tool at the Bio-Analytic Resource for Plant Biology (BAR) public database (https://bar.utoronto.ca/), expressed in GeneChip Operating System (GCOS) units (scale 0-10,000).

Data S2. List of genes from the RNAseq analysis generated from the comparison of *atg7* vs Col-0 imbibed seeds at 24 hoi.

Data S3. GSEA (*p*-value = 0.05) carried out on the list of genes from the RNAseq analysis generated from the comparison of *atg7* vs Col-0 imbibed seeds at 24 hoi. Lipid storage, seed maturation, and response to endoplasmic reticulum stress categories are highlighted in red. Genes that belong to selected categories are listed in the second worksheet, and those meeting the cut-offs (p-adj $\leq$ 0.05 and $Log_2FC \leq 2.0$) are highlighted in green.

Data S4. List of genes from the RNAseq analysis that respond to the presence of ABA in *atg7* seeds. DEG differentially regulated in *atg7* seeds, comparing 96 hoi in the presence of ABA vs 48 hoi in the absence. Selected DEG meet the cut-offs of p-adj $\leq$ 0.05 and $Log_2FC \leq 2.0$.

Data S5. List of genes from the RNAseq analysis that respond to the presence of ABA in WT seeds. DEG differentially regulated in WT seeds, comparing 96 hoi in the presence of ABA vs 48 hoi in the absence. Selected DEG meet the cut-offs of p-adj $\leq$ 0.05 and $Log_2FC \leq 2.0$.

Data S6. List of genes from the Venn diagram**.**

Data S7. List of DEG showing opposite expression patterns in WT and in *atg7* in response to ABA (96 hoi in the presence of ABA vs 48 hoi in the absence) and enrichment analysis performed on these DEG (worksheets 2 and 3).

Data S8. List of DEG showing opposite expression patterns in WT and in *atg7* in response to ABA (96 hoi in the presence of ABA vs 48 hoi in the absence) and their expression in siliques and seeds retrieved from the Gene Expression Tool available at the Bio-Analytic Resource for Plant Biology (BAR) public database (https://bar.utoronto.ca/).

Figure 1

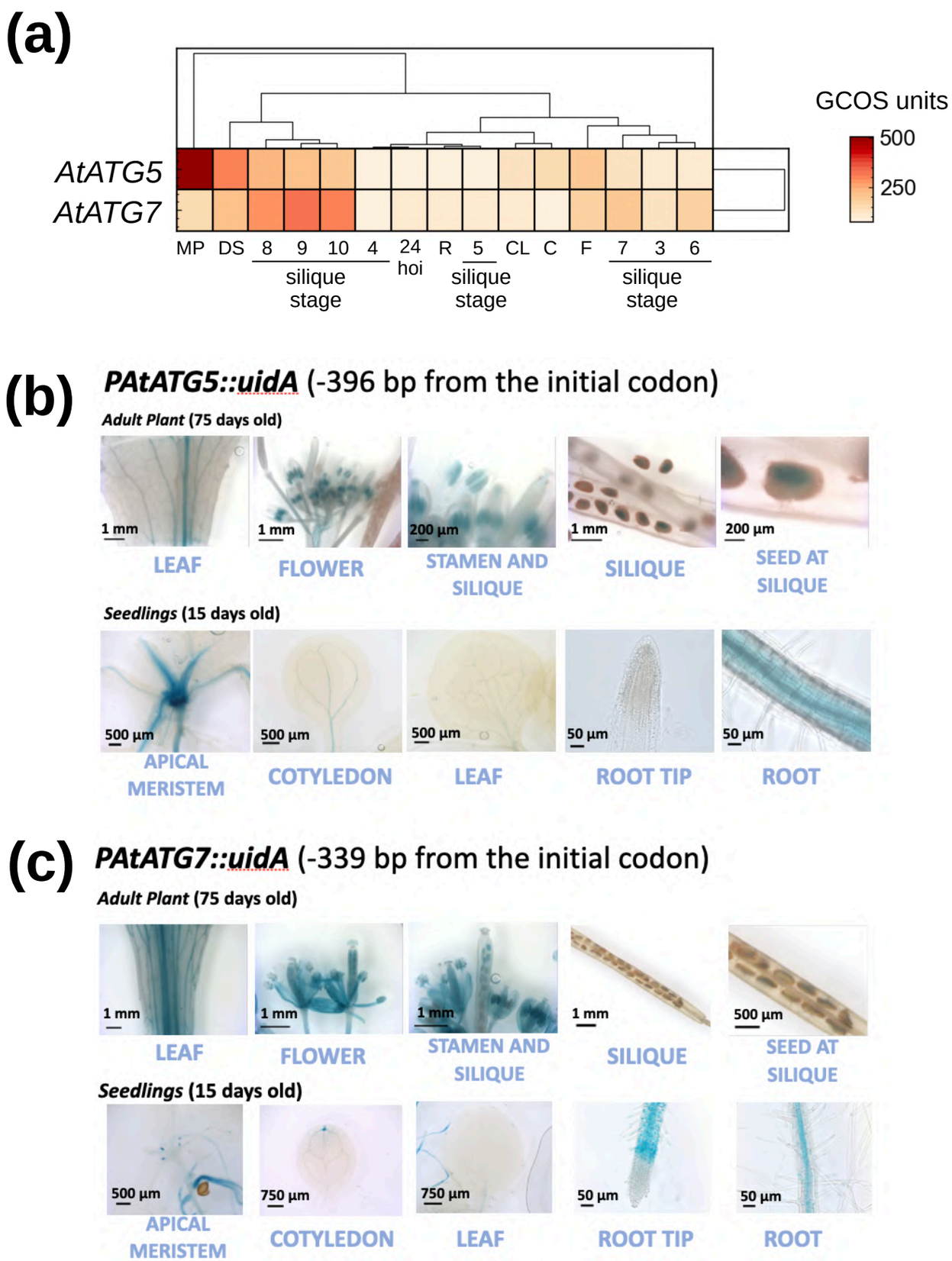
(a)
AtATG5
AtATG7
MP DS 8 9 10 4 24 hoi R 5 CL C F 7 3 6
silique stage
silique stage
silique stage
GCOS units
500
250
(b)
PAtATG5::uidA (-396 bp from the initial codon)
Adult Plant (75 days old)
1 mm
1 mm
200 µm
1 mm
200 µm
LEAF
FLOWER
STAMEN AND SILIQUE
SILIQUE
SEED AT SILIQUE
Seedlings (15 days old)
500 µm
500 µm
500 µm
50 µm
50 µm
APICAL MERISTEM
COTYLEDON
LEAF
ROOT TIP
ROOT
(c)
PAtATG7::uidA (-339 bp from the initial codon)
Adult Plant (75 days old)
1 mm
1 mm
1 mm
1 mm
500 µm
LEAF
FLOWER
STAMEN AND SILIQUE
SILIQUE
SEED AT SILIQUE
Seedlings (15 days old)
500 µm
750 µm
750 µm
50 µm
50 µm
APICAL MERISTEM
COTYLEDON
LEAF
ROOT TIP
ROOT

Figure 2

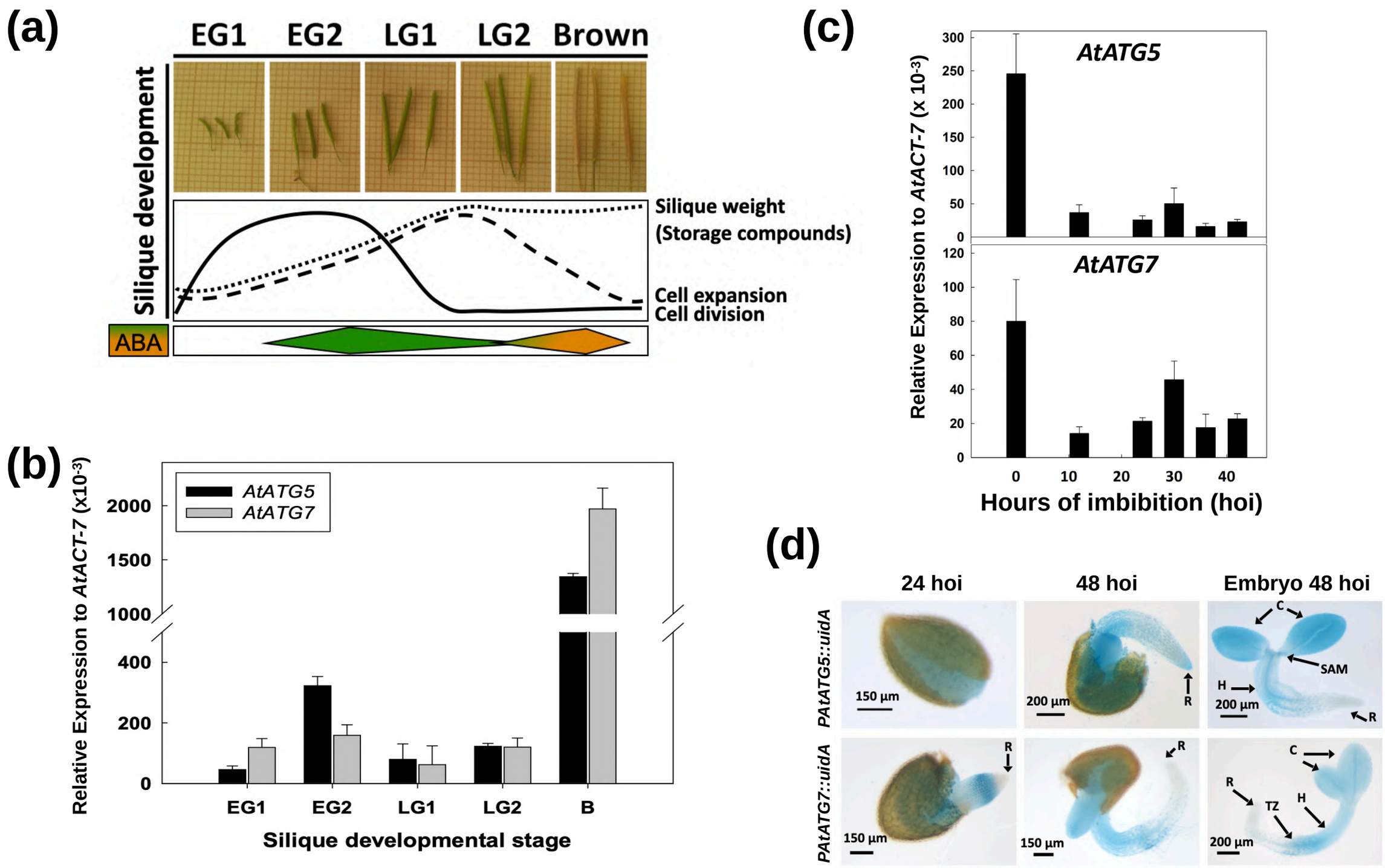
(a)
EG1
EG2
LG1
LG2
Brown
Silique development
Silique weight
(Storage compounds)
Cell expansion
Cell division
ABA
(b)
AtATG5
AtATG7
Relative Expression to AtACT-7 (x10-3)
2000
1500
1000
400
200
0
EG1
EG2
LG1
LG2
B
Silique developmental stage
(c)
AtATG5
AtATG7
Relative Expression to AtACT-7 (x 10-3)
300
250
200
150
100
50
0
120
100
80
60
40
20
0
0
10
20
30
40
Hours of imbibition (hoi)
(d)
24 hoi
48 hoi
Embryo 48 hoi
PAtATG5::uidA
PAtATG7::uidA
150 µm
200 µm
R
C
SAM
H
TZ

Figure 3

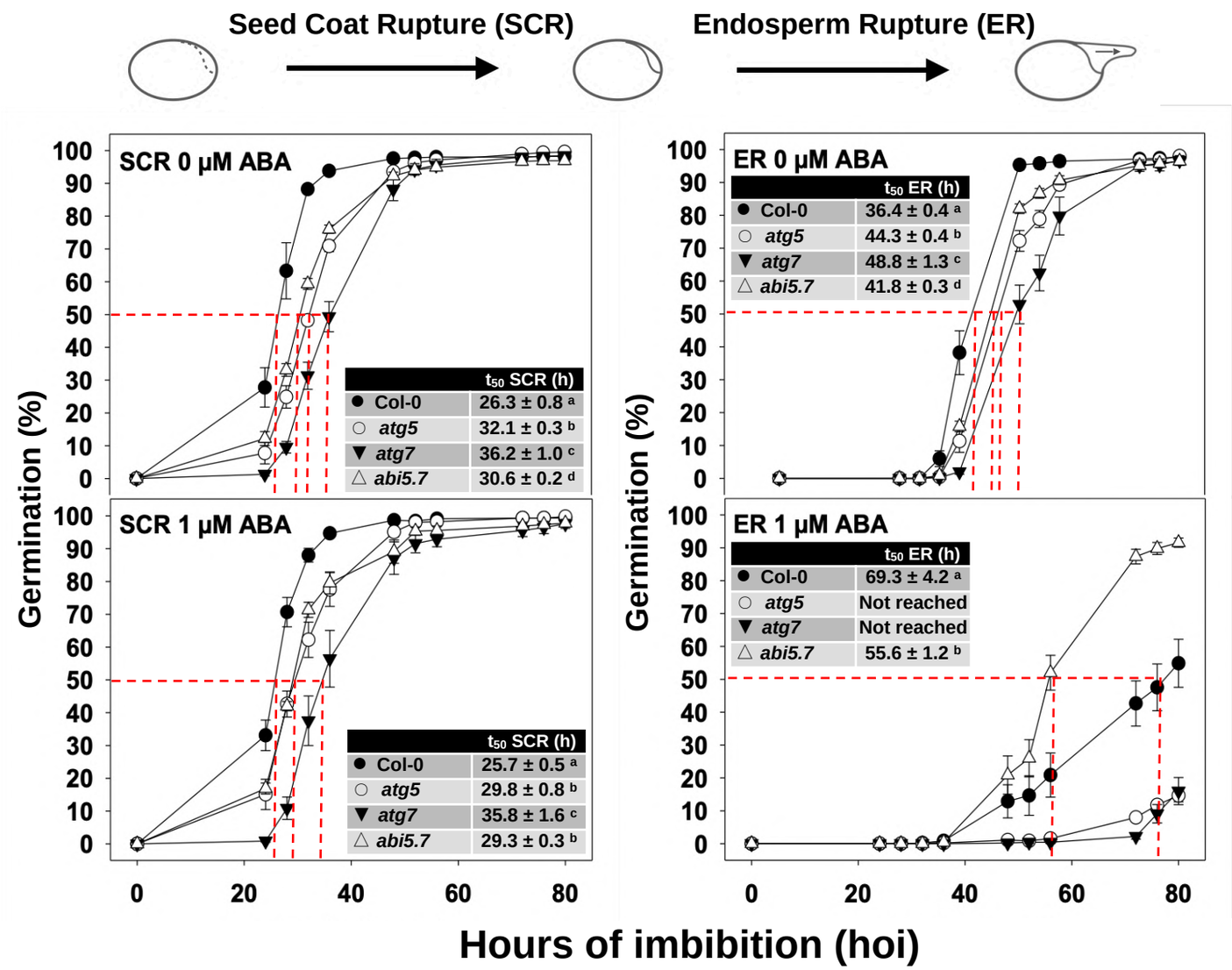
Seed Coat Rupture (SCR)
Endosperm Rupture (ER)
SCR 0 µM ABA
t50 SCR (h)
Col-0 26.3 ± 0.8 a
atg5 32.1 ± 0.3 b
atg7 36.2 ± 1.0 c
abi5.7 30.6 ± 0.2 d
SCR 1 µM ABA
t50 SCR (h)
Col-0 25.7 ± 0.5 a
atg5 29.8 ± 0.8 b
atg7 35.8 ± 1.6 c
abi5.7 29.3 ± 0.3 b
ER 0 µM ABA
t50 ER (h)
Col-0 36.4 ± 0.4 a
atg5 44.3 ± 0.4 b
atg7 48.8 ± 1.3 c
abi5.7 41.8 ± 0.3 d
ER 1 µM ABA
t50 ER (h)
Col-0 69.3 ± 4.2 a
atg5 Not reached
atg7 Not reached
abi5.7 55.6 ± 1.2 b
Germination (%)
Hours of imbibition (hoi)

Figure 4

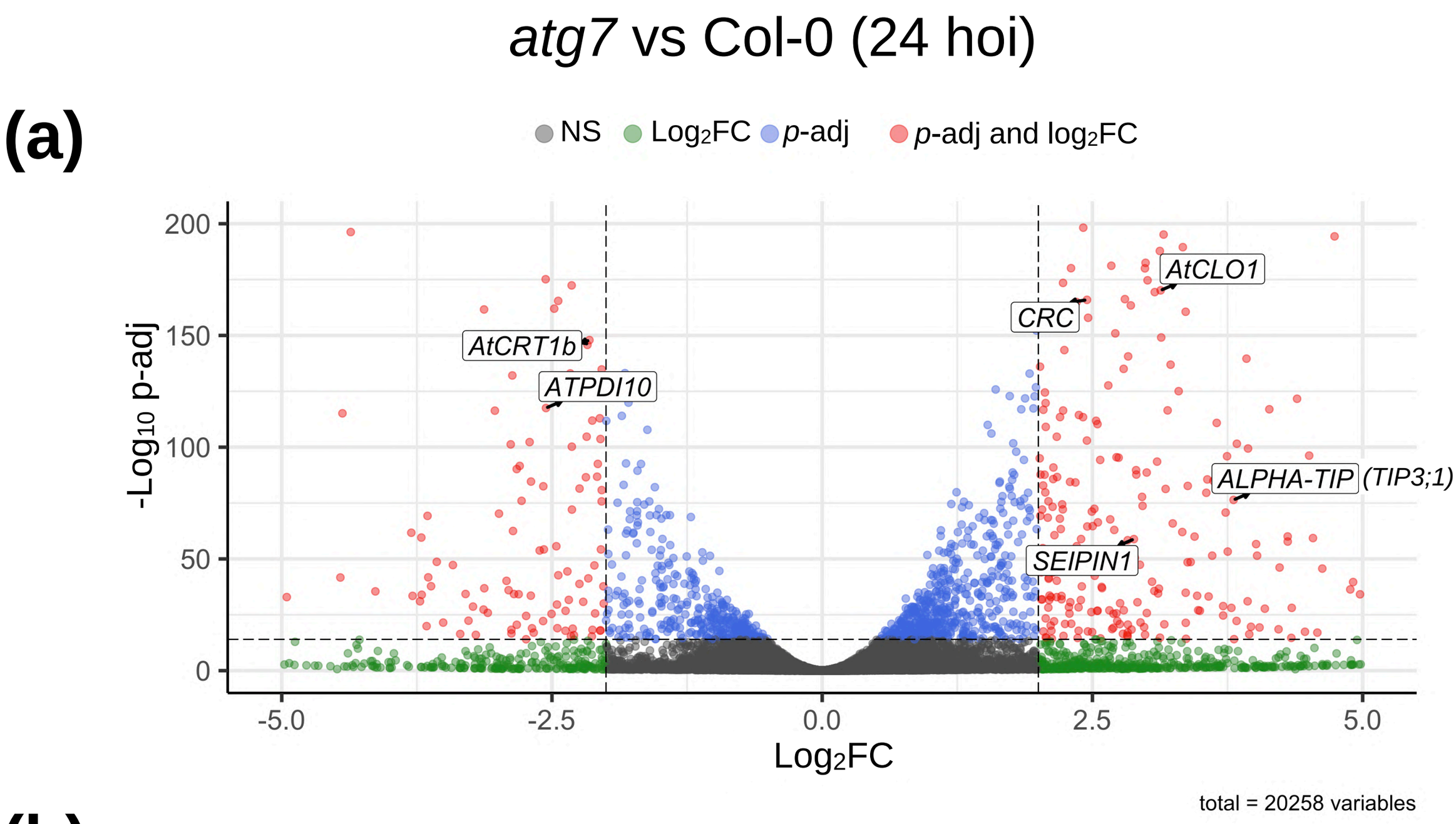
(a)
atg7 vs Col-0 (24 hoi)
NS
Log2FC
p-adj
p-adj and log2FC
-Log10 p-adj
Log2FC
AtCRT1b
ATPDI10
CRC
AtCLO1
ALPHA-TIP (TIP3;1)
SEIPIN1
total = 20258 variables

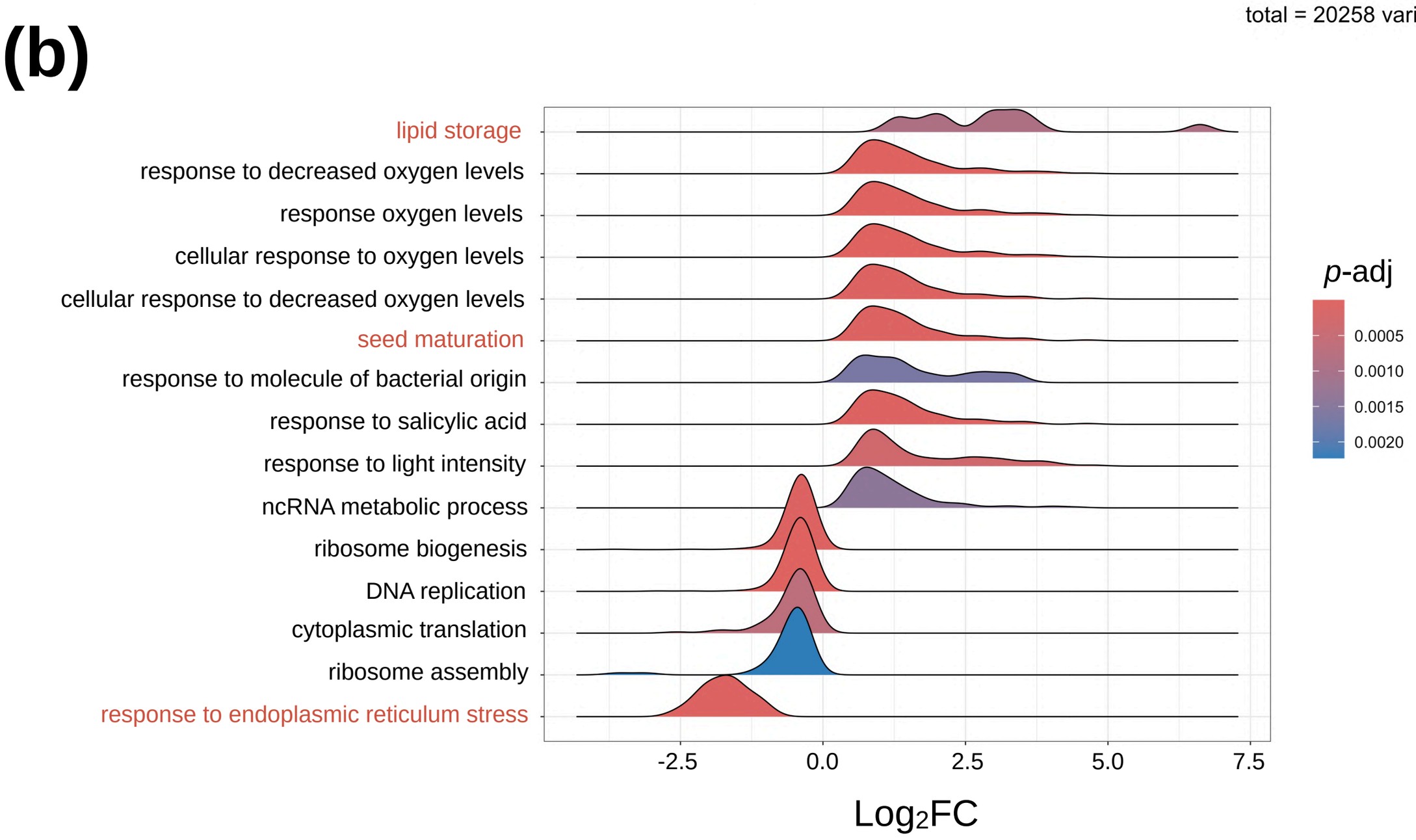
(b)
lipid storage
response to decreased oxygen levels
response oxygen levels
cellular response to oxygen levels
cellular response to decreased oxygen levels
seed maturation
response to molecule of bacterial origin
response to salicylic acid
response to light intensity
ncRNA metabolic process
ribosome biogenesis
DNA replication
cytoplasmic translation
ribosome assembly
response to endoplasmic reticulum stress
Log2FC
p-adj
0.0005
0.0010
0.0015
0.0020

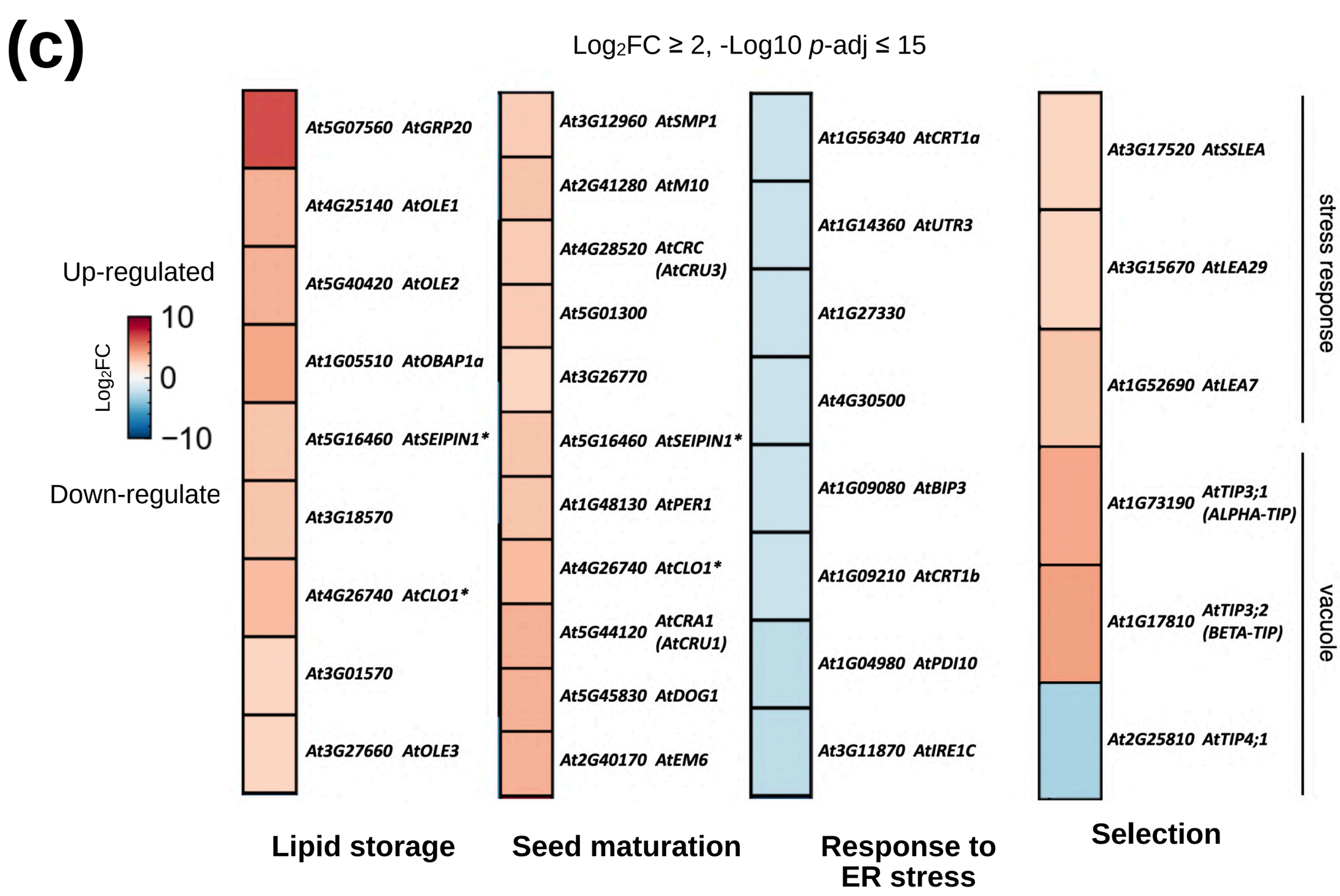
(c)
Log2FC ≥ 2, -Log10 p-adj ≤ 15
Up-regulated
Log2FC
10
0
−10
Down-regulate
At5G07560 AtGRP20
At4G25140 AtOLE1
At5G40420 AtOLE2
At1G05510 AtOBAP1a
At5G16460 AtSEIPIN1*
At3G18570
At4G26740 AtCLO1*
At3G01570
At3G27660 AtOLE3
At3G12960 AtSMP1
At2G41280 AtM10
At4G28520 AtCRC (AtCRU3)
At5G01300
At3G26770
At5G16460 AtSEIPIN1*
At1G48130 AtPER1
At4G26740 AtCLO1*
At5G44120 AtCRA1 (AtCRU1)
At5G45830 AtDOG1
At2G40170 AtEM6
At1G56340 AtCRT1a
At1G14360 AtUTR3
At1G27330
At4G30500
At1G09080 AtBIP3
At1G09210 AtCRT1b
At1G04980 AtPDI10
At3G11870 AtIRE1C
At3G17520 AtSSLEA
At3G15670 AtLEA29
At1G52690 AtLEA7
At1G73190 AtTIP3;1 (ALPHA-TIP)
At1G17810 AtTIP3;2 (BETA-TIP)
At2G25810 AtTIP4;1
stress response
vacuole
Lipid storage
Seed maturation
Response to ER stress
Selection

Figure 5

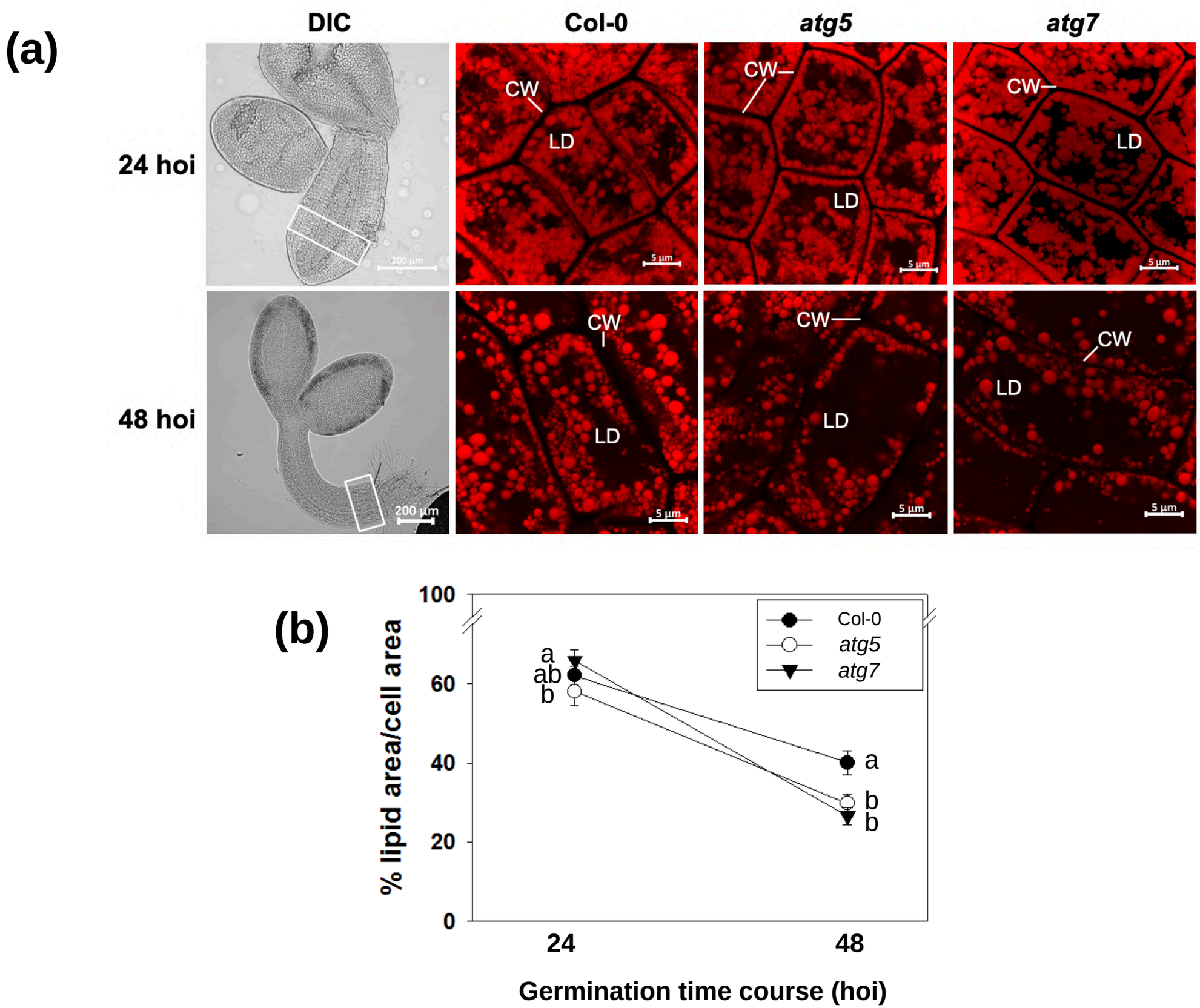
(a)
DIC
Col-0
atg5
atg7
24 hoi
48 hoi
CW
LD
200 µm
5 µm
(b)
% lipid area/cell area
Germination time course (hoi)
Col-0
atg5
atg7
100
60
40
20
0
24
48
a
ab
b
a
b
b

Figure 6

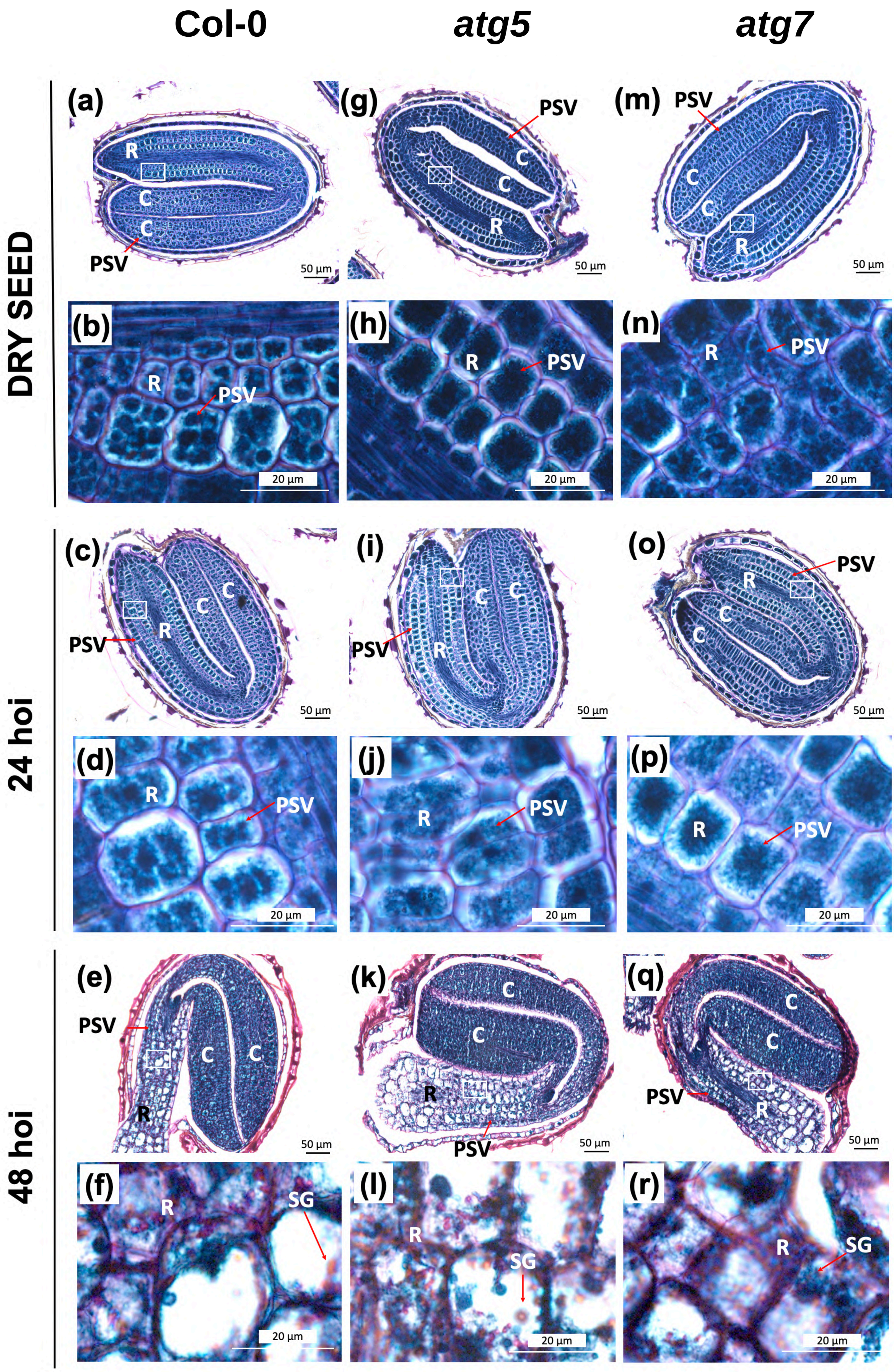
Col-0
atg5
atg7
DRY SEED
24 hoi
48 hoi
(a)
(b)
(c)
(d)
(e)
(f)
(g)
(h)
(i)
(j)
(k)
(l)
(m)
(n)
(o)
(p)
(q)
(r)
R
C
PSV
SG
50 µm
20 µm

Figure 7

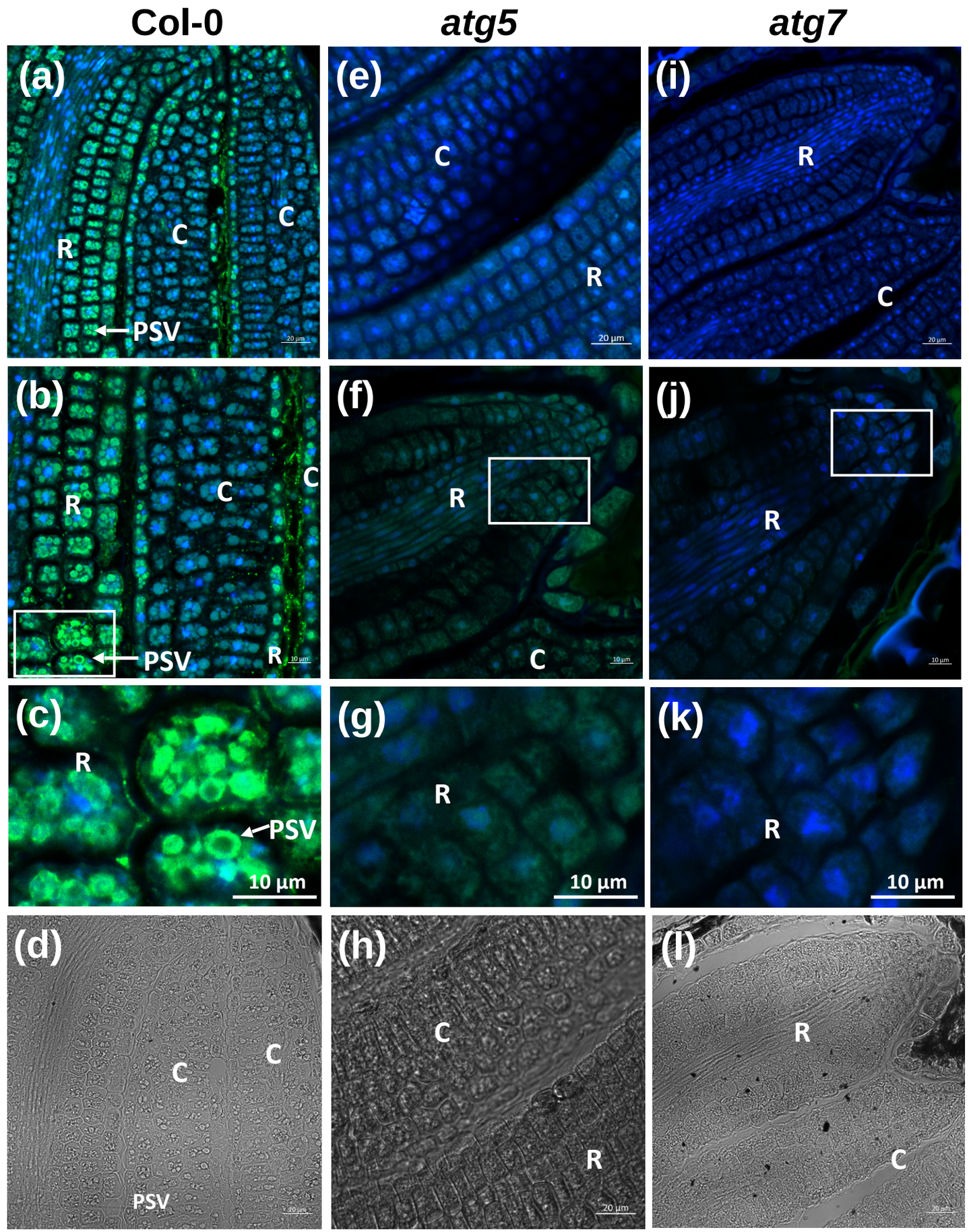

Figure 8

(a)

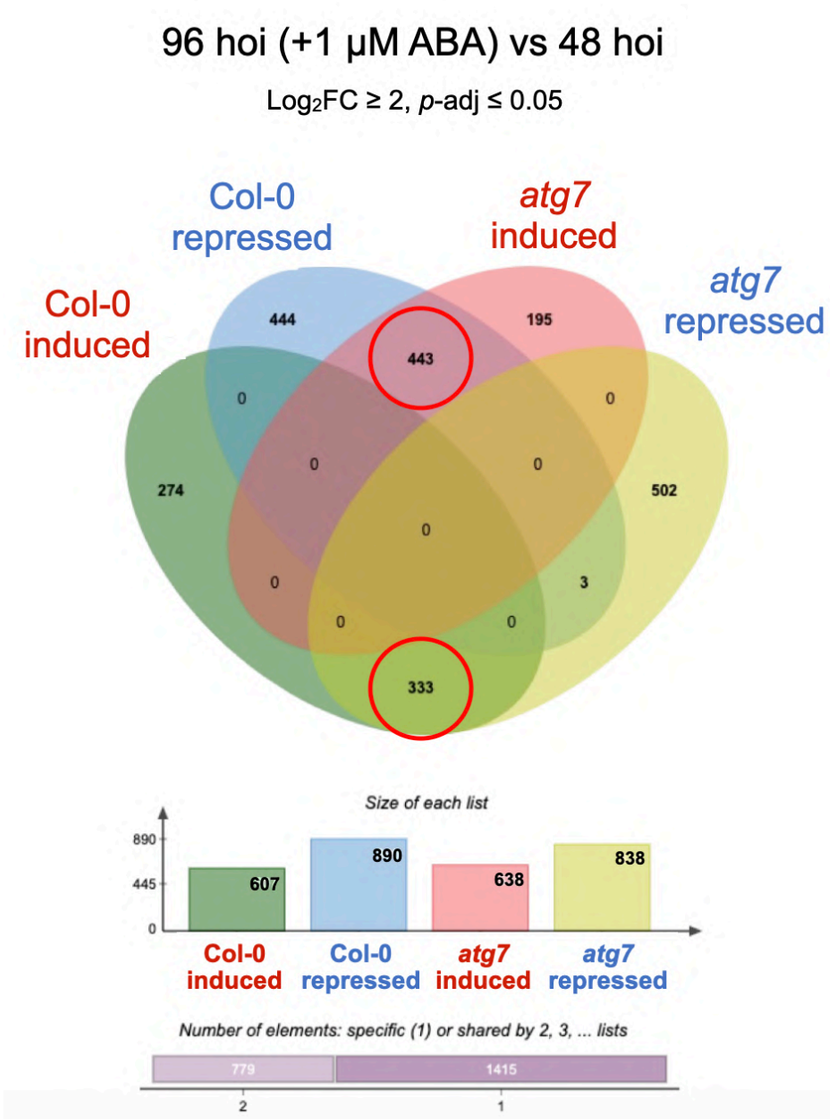

(b)

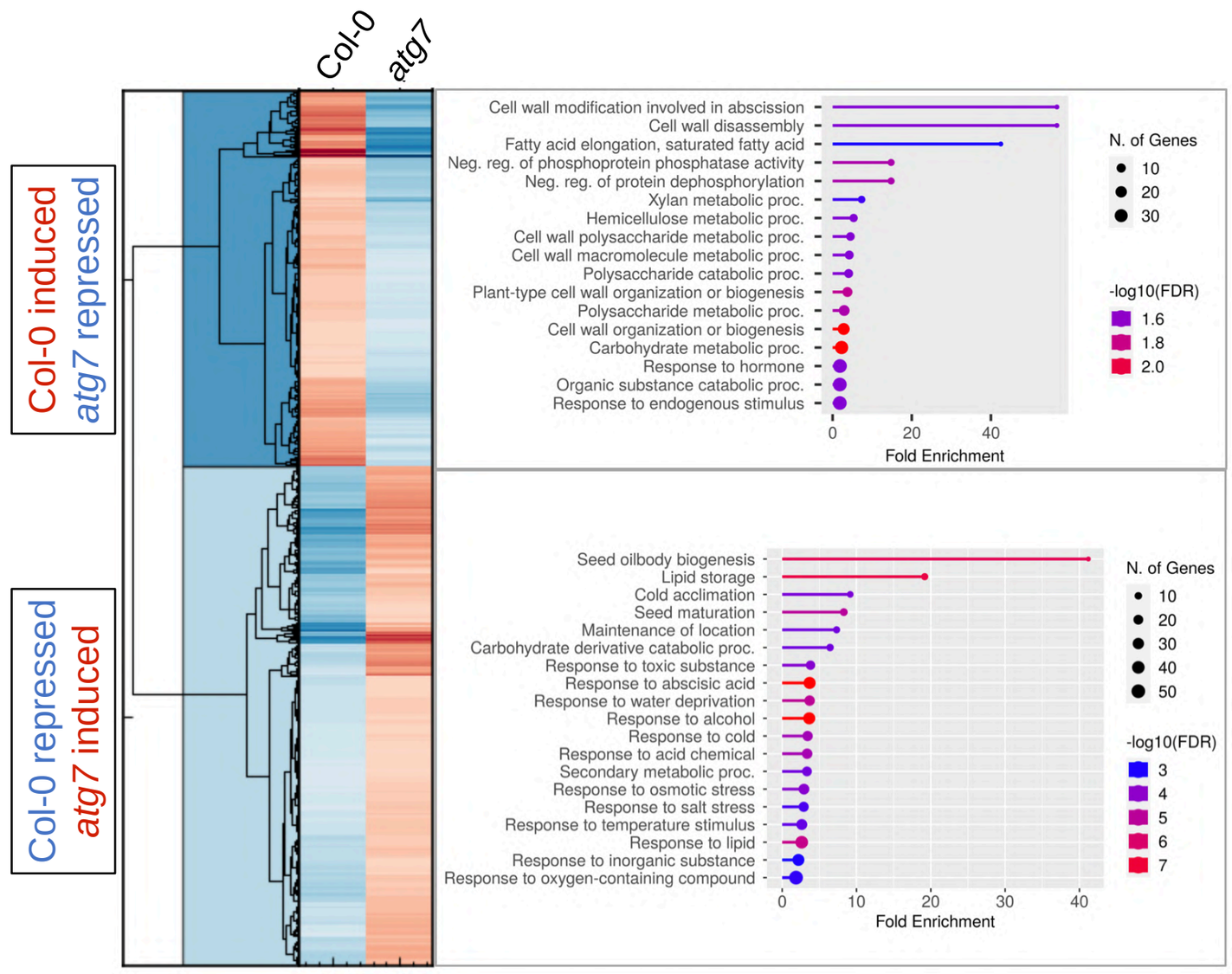

(c)

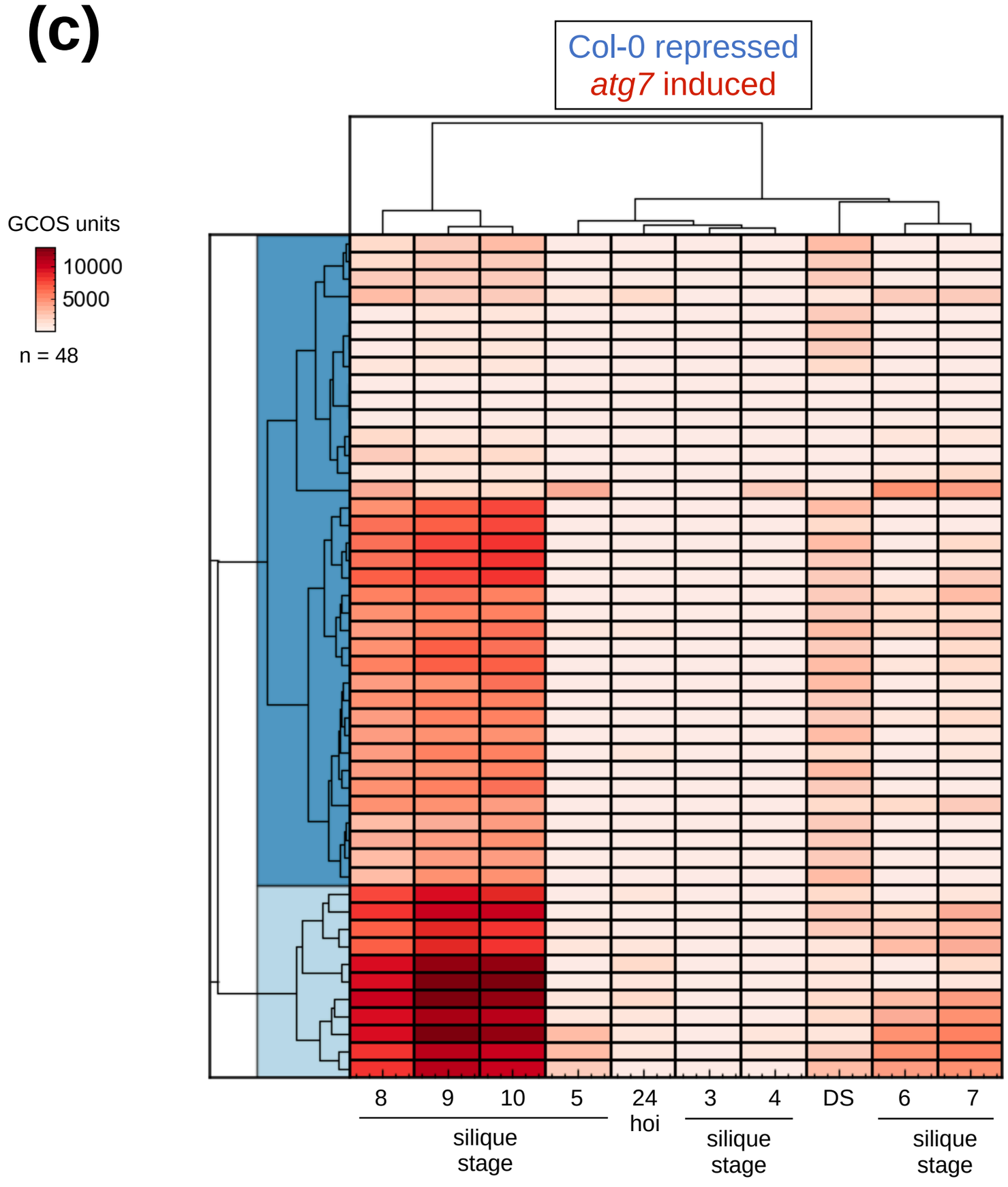

Gene	Alias	Function	Putative target for
AT3G15280		Hypothetical protein	ABI3
AT1G72100		Late embryogenesis abundant	ABI3,ABI5
AT5G45310		Carboxylic acid metabolic process	ABI3
AT2G31980	AtCYS2	Inhibitor of cysteine proteinases	ABI3
AT4G36700		RmlC-like cupin	ABI3, ABI5
AT4G36600		Late embryogenesis abundant	ABI3,ABI5
AT5G18450		Integrase-type DNA-binding protein	ABI3
AT5G50170		C2 calcium/lipid-binding	ABI3
AT4G05100	AtMYB74	MYB domain transcription factor 74	ABI5
AT4G35690		Cell wall biogenesis/organization	ABI3
AT5G46350	ATWRKY8	WRKY transcription factor	ABI3
AT2G41070	ATBZIP12	Transcription factor homologous to ABI5	ABI3
AT2G19320		Hypothetical protein	ABI3,ABI5
AT5G09640	SCPL19	Serine carboxypeptidase	ABI3
AT5G51210	OLEO3	Seed lipid storage	ABI3
AT2G40170	ATEM6	Late embryogenesis abundant	ABI3,ABI5
AT2G42560	LEA25	Late embryogenesis abundant	ABI3
AT3G17520	SSLEA	Late embryogenesis abundant	ABI5
AT2G47770	ATTSPO	Trp-rich sensory protein	ABI3,ABI5
AT5G45690		Histone acetyltransferase	ABI3
AT2G38905		Low temperature and salt responsive	ABI3
AT5G01300		Phosphatidylethanolamine-binding	ABI3,ABI5
AT3G54940		Papain family cysteine protease	ABI3,ABI5
AT4G21020		Late embryogenesis abundant	ABI3
AT5G01670		NAD(P)-linked oxidoreductase superfamily	ABI5
AT5G07330		Hypothetical protein	ABI3
AT2G21820		Seed maturation protein	ABI3,ABI5
AT5G22470	AtPARP3	Poly(ADP-ribose) polymerase 3	ABI3
AT1G27990		Transmembrane protein	ABI3,ABI5
AT5G62490	ATHVA22B	ABA/stress-induced protein	ABI3,ABI5
AT3G51810	AT3	Late embryogenesis abundant	ABI3
AT3G12960	SMP1	Seed maturation protein 1	ABI3
AT4G31830		Protein coding	ABI3
AT3G53040		Late embryogenesis abundant	ABI3
AT1G02700		GATA transcription factor-like protein	ABI3,ABI5
AT4G09600	GASA3	Related to GA-stimulated transcript	ABI3,ABI5
AT5G52300	LTI65	Responsive to desiccation	ABI5
AT1G54870	ChlADR	Chloroplast aldehyde reductase	ABI3,ABI5
AT1G05510	OBAP1a	Oil body associated protein	ABI3,ABI5
AT2G02120	LCR70	Defensin	ABI3
AT1G48130	ATPER1	Cysteine peroxiredoxin	ABI3,ABI5
AT3G15670	LEA29	Late embryogenesis abundant	ABI3,ABI5
AT5G66400	ATDI8	Dehydrin protein family	ABI5
AT5G54740	SESA5	Seed storage albumin	ABI3
AT1G04560		Related to freezing tolerance	ABI5
AT4G25140	OLE1	Seed lipid accumulation	ABI3,ABI5
AT5G40420	OLE2	Seed lipid accumulation	ABI3,ABI5
AT2G28490		RmlC-like cupin	ABI3

Figure 9

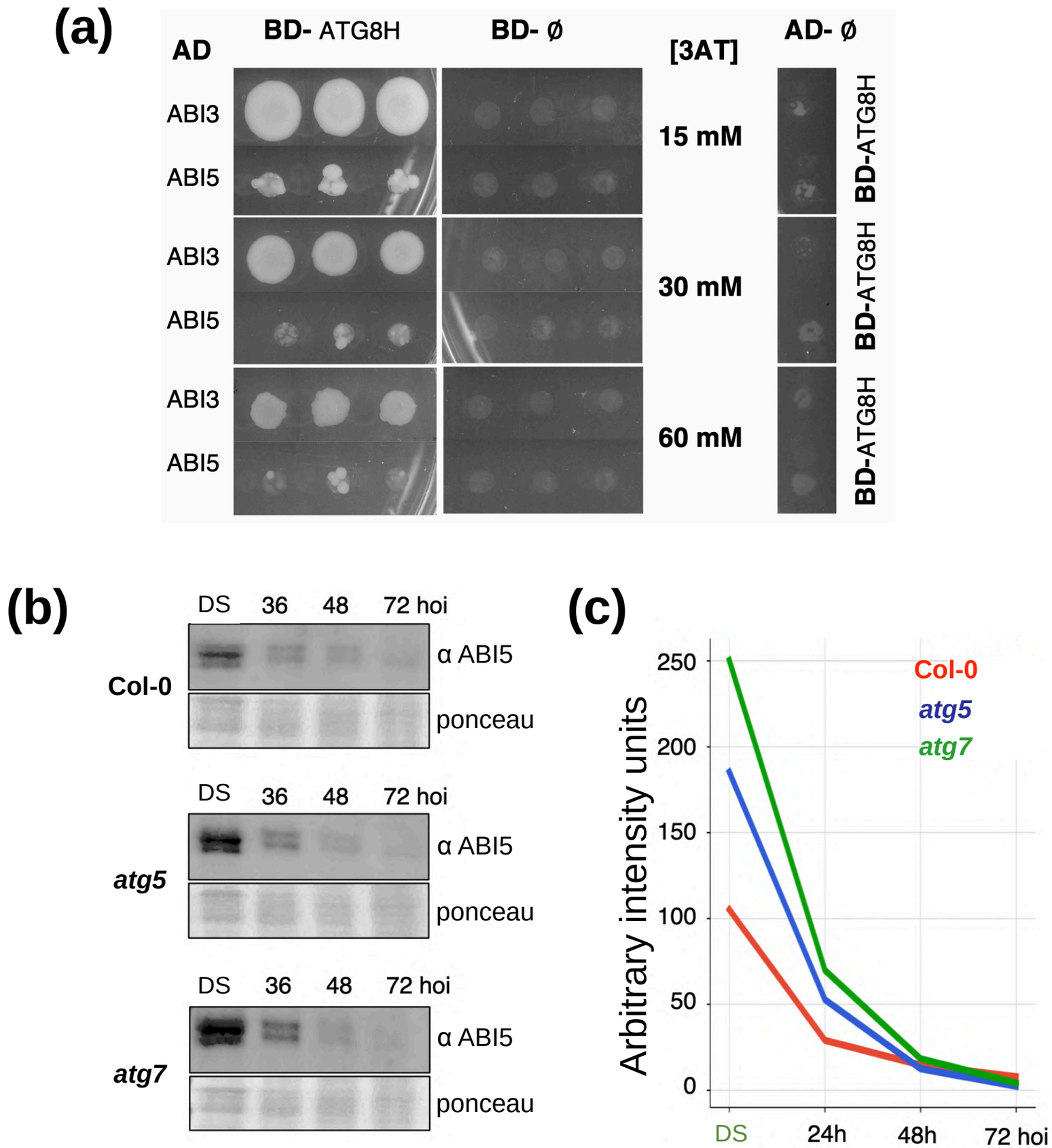
(a)
AD
BD- ATG8H
BD- Ø
[3AT]
AD- Ø
ABI3
ABI5
15 mM
30 mM
60 mM
BD-ATG8H
(b)
DS
36
48
72 hoi
Col-0
atg5
atg7
α ABI5
ponceau
(c)
Arbitrary intensity units
250
200
150
100
50
0
Col-0
atg5
atg7
DS
24h
48h
72 hoi

Figure 10

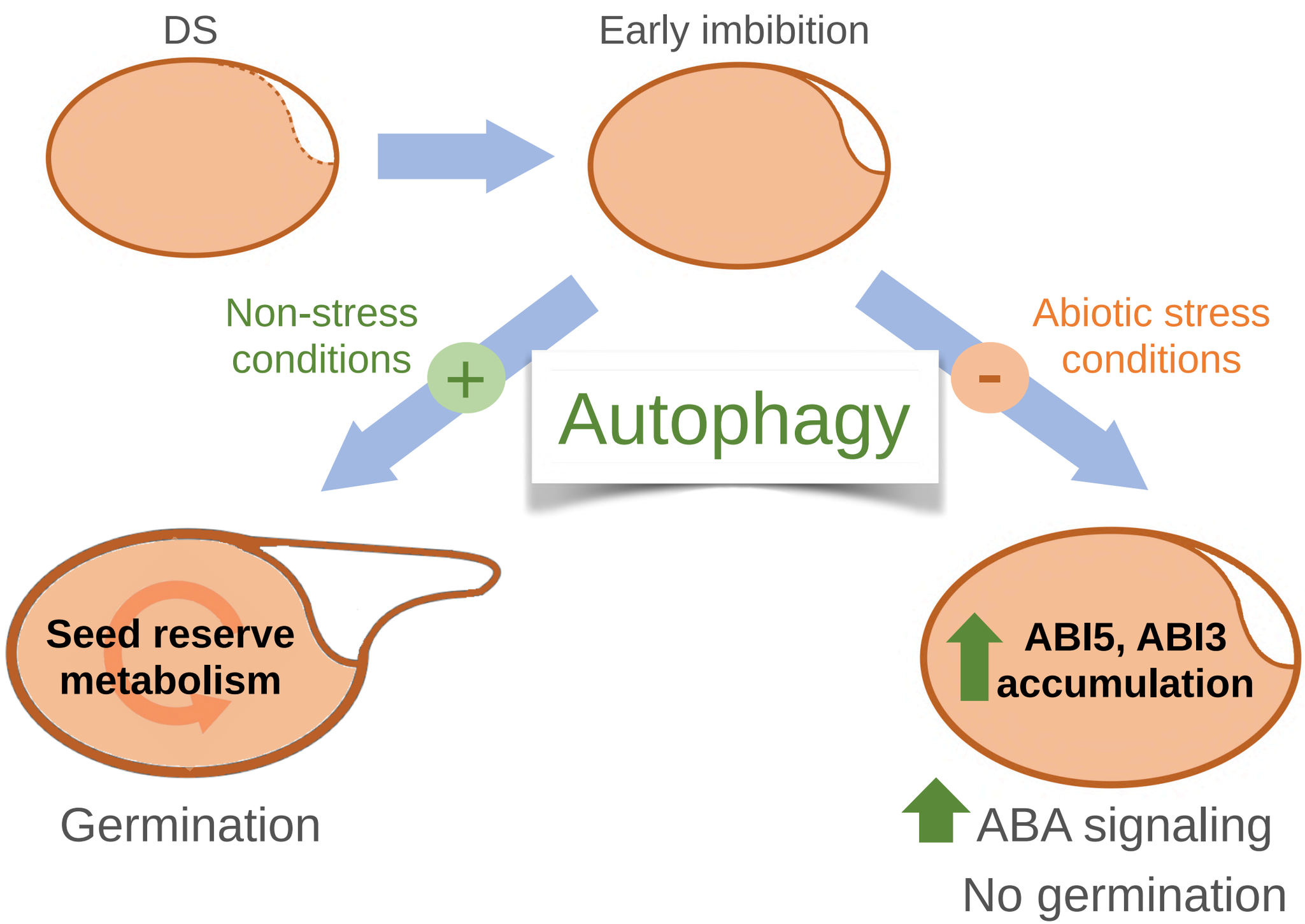
DS
Early imbibition
Non-stress conditions
+
Autophagy
-
Abiotic stress conditions
Seed reserve metabolism
Germination
ABI5, ABI3 accumulation
ABA signaling
No germination

Figure S1

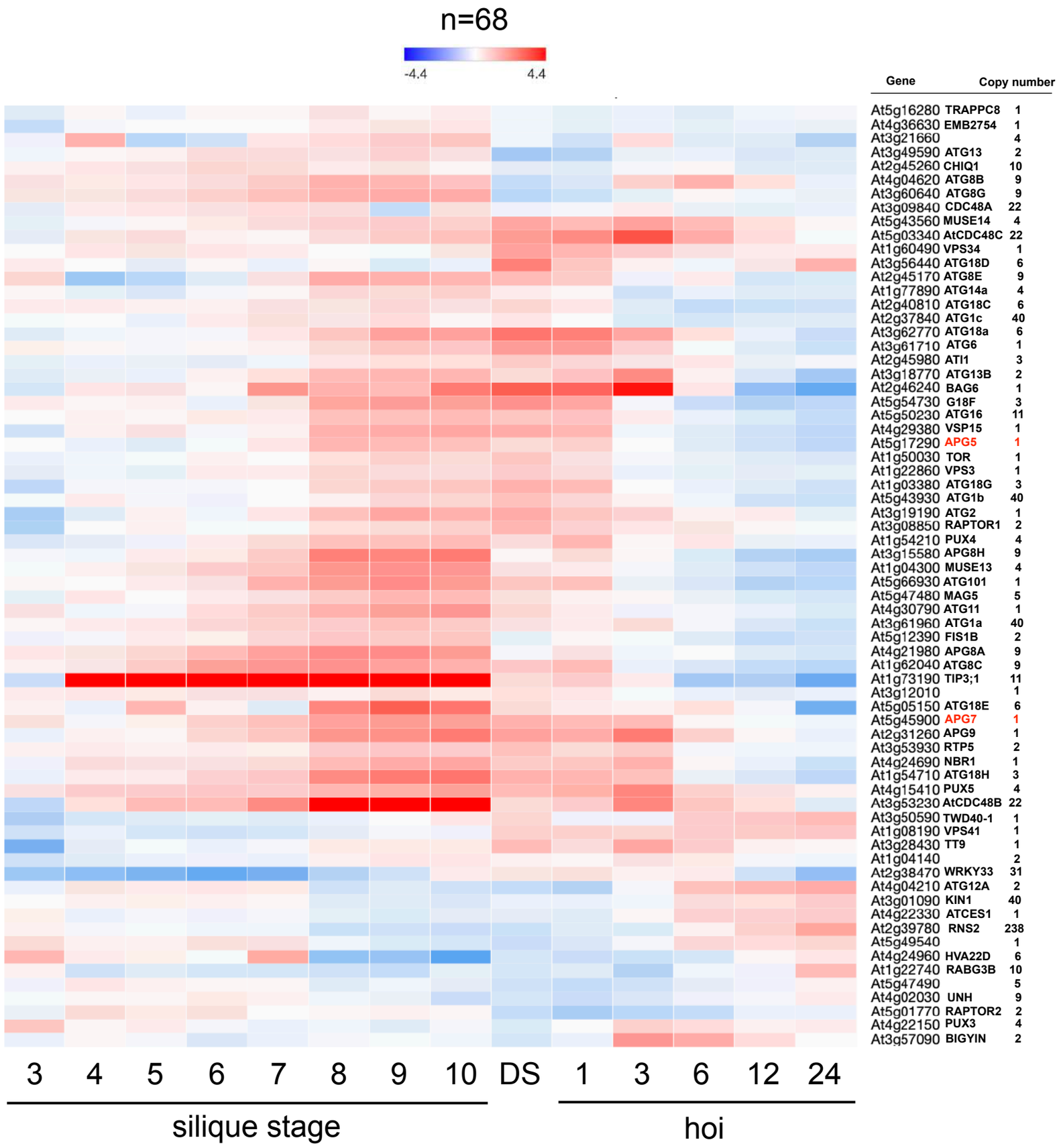
n=68
-4.4
4.4
Gene
Copy number
At5g16280 TRAPPC8 1
At4g36630 EMB2754 1
At3g21660 4
At3g49590 ATG13 2
At2g45260 CHIQ1 10
At4g04620 ATG8B 9
At3g60640 ATG8G 9
At3g09840 CDC48A 22
At5g43560 MUSE14 4
At5g03340 AtCDC48C 22
At1g60490 VPS34 1
At3g56440 ATG18D 6
At2g45170 ATG8E 9
At1g77890 ATG14a 4
At2g40810 ATG18C 6
At2g37840 ATG1c 40
At3g62770 ATG18a 6
At3g61710 ATG6 1
At2g45980 ATI1 3
At3g18770 ATG13B 2
At2g46240 BAG6 1
At5g54730 G18F 3
At5g50230 ATG16 11
At4g29380 VSP15 1
At5g17290 APG5 1
At1g50030 TOR 1
At1g22860 VPS3 1
At1g03380 ATG18G 3
At5g43930 ATG1b 40
At3g19190 ATG2 1
At3g08850 RAPTOR1 2
At1g54210 PUX4 4
At3g15580 APG8H 9
At1g04300 MUSE13 4
At5g66930 ATG101 1
At5g47480 MAG5 5
At4g30790 ATG11 1
At3g61960 ATG1a 40
At5g12390 FIS1B 2
At4g21980 APG8A 9
At1g62040 ATG8C 9
At1g73190 TIP3;1 11
At3g12010 1
At5g05150 ATG18E 6
At5g45900 APG7 1
At2g31260 APG9 1
At3g53930 RTP5 2
At4g24690 NBR1 1
At1g54710 ATG18H 3
At4g15410 PUX5 4
At3g53230 AtCDC48B 22
At3g50590 TWD40-1 1
At1g08190 VPS41 1
At3g28430 TT9 1
At1g04140 2
At2g38470 WRKY33 31
At4g04210 ATG12A 2
At3g01090 KIN1 40
At4g22330 ATCES1 1
At2g39780 RNS2 238
At5g49540 1
At4g24960 HVA22D 6
At1g22740 RABG3B 10
At5g47490 5
At4g02030 UNH 9
At5g01770 RAPTOR2 2
At4g22150 PUX3 4
At3g57090 BIGYIN 2
3 4 5 6 7 8 9 10 DS 1 3 6 12 24
silique stage
hoi

Figure S2

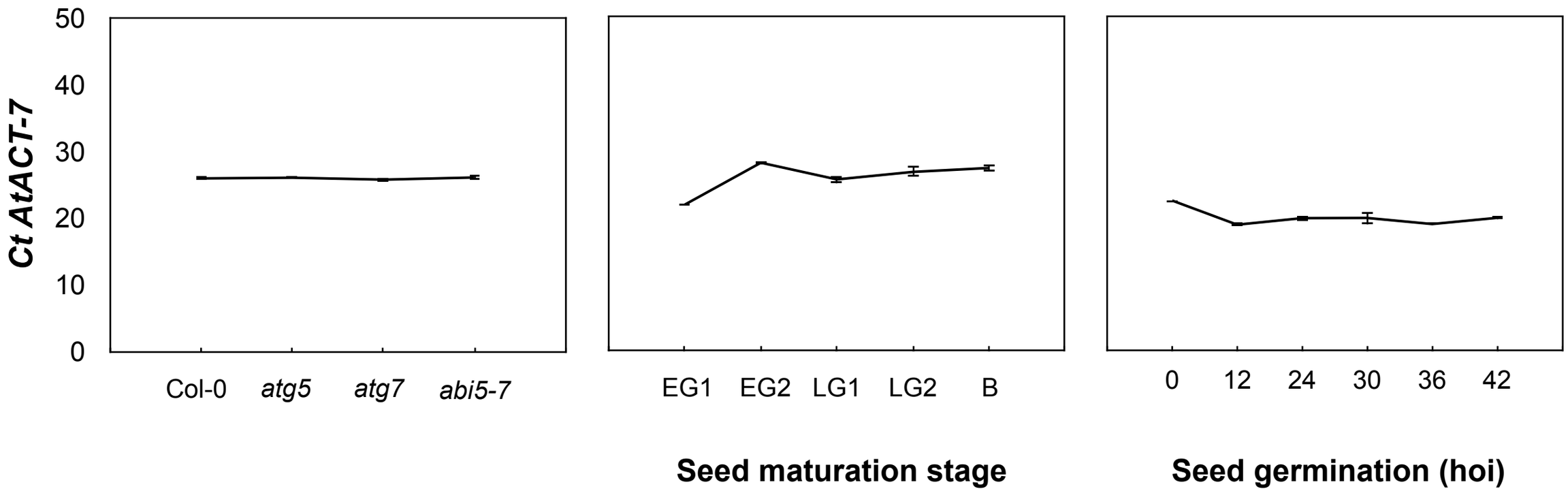
Ct AtACT-7
50
40
30
20
10
0
Col-0
atg5
atg7
abi5-7
EG1
EG2
LG1
LG2
B
Seed maturation stage
0
12
24
30
36
42
Seed germination (hoi)

Figure S3

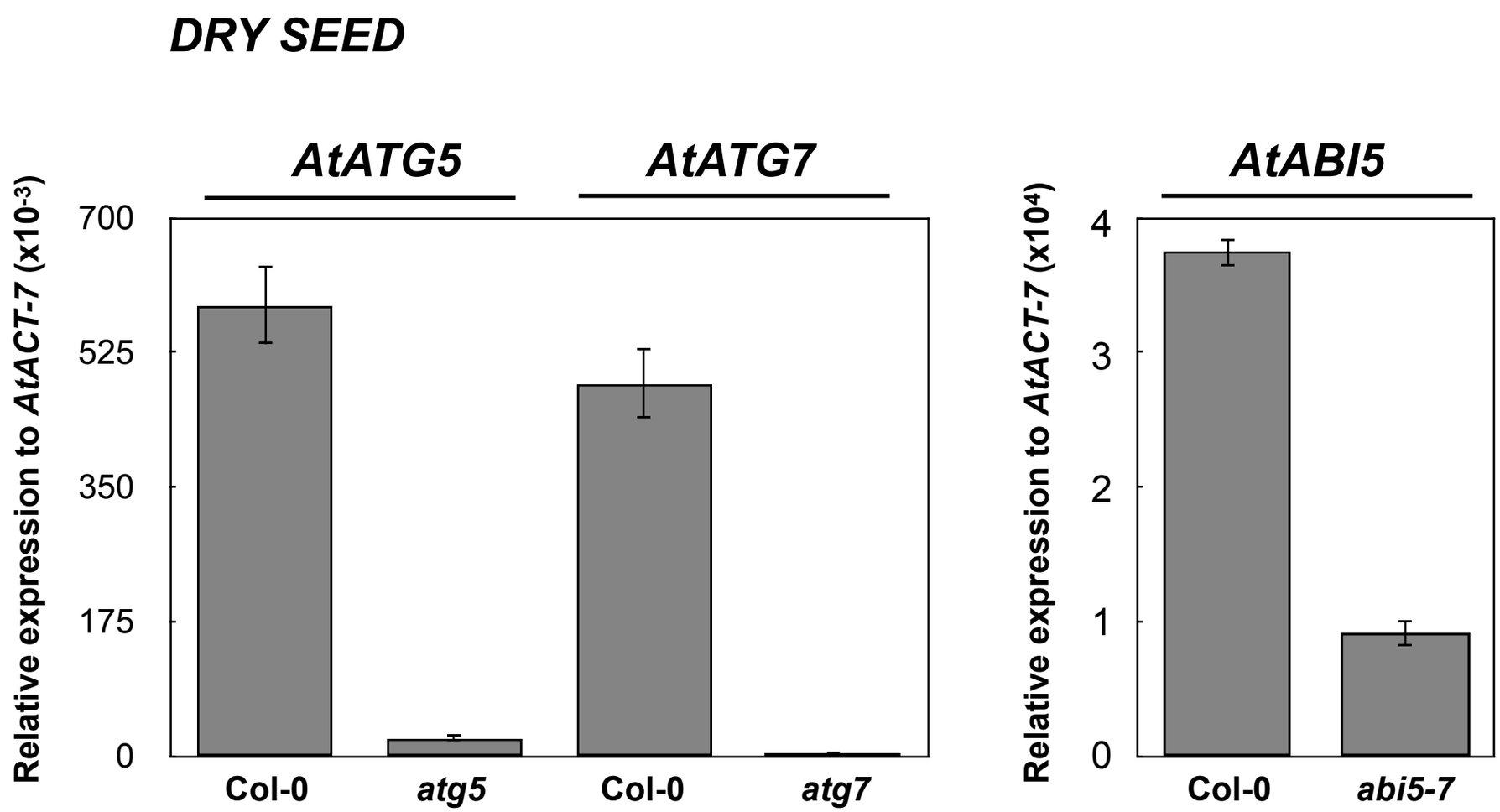
DRY SEED
AtATG5
AtATG7
AtABI5
Relative expression to AtACT-7 (x10-3)
700
525
350
175
0
Col-0
atg5
Col-0
atg7
Relative expression to AtACT-7 (x104)
4
3
2
1
0
Col-0
abi5-7

Figure S4

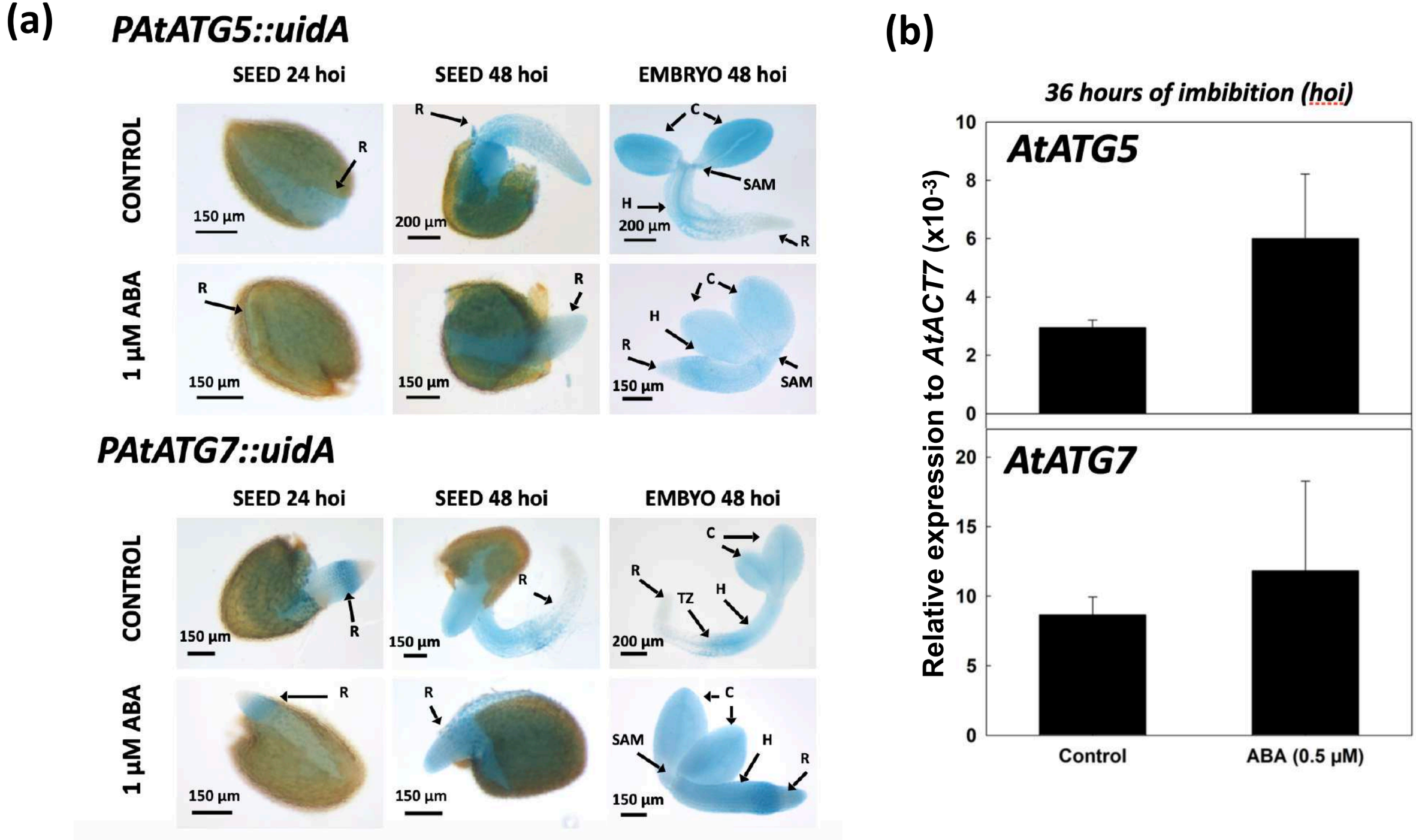
(a)
PAtATG5::uidA
SEED 24 hoi
SEED 48 hoi
EMBRYO 48 hoi
CONTROL
1 µM ABA
R
C
SAM
H
TZ
150 µm
200 µm
PAtATG7::uidA
SEED 24 hoi
SEED 48 hoi
EMBYO 48 hoi
CONTROL
1 µM ABA
R
C
TZ
H
SAM
150 µm
200 µm
(b)
36 hours of imbibition (hoi)
AtATG5
AtATG7
Relative expression to AtACT7 (x10-3)
Control
ABA (0.5 µM)

Figure S5

(a)

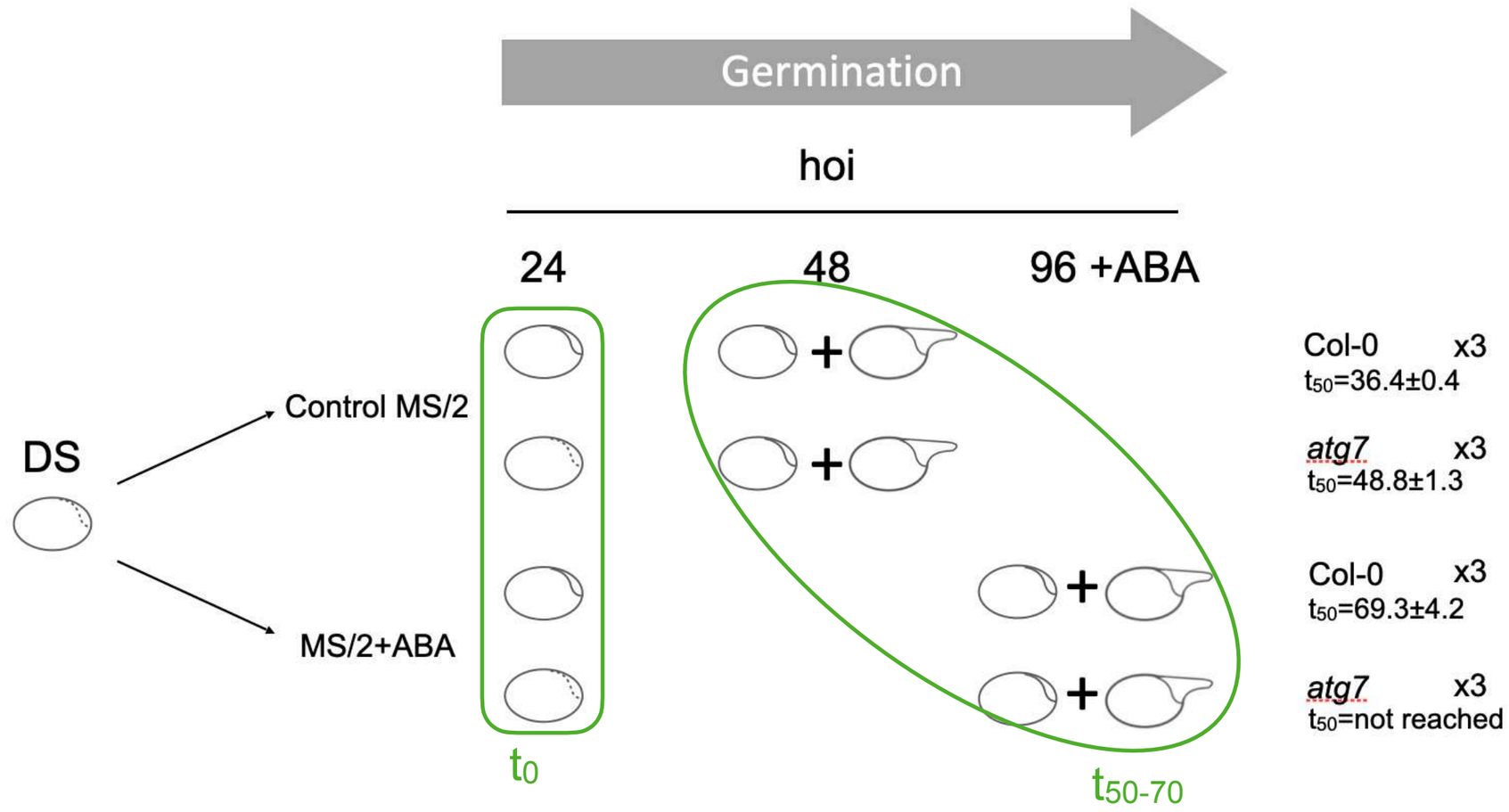

(b)

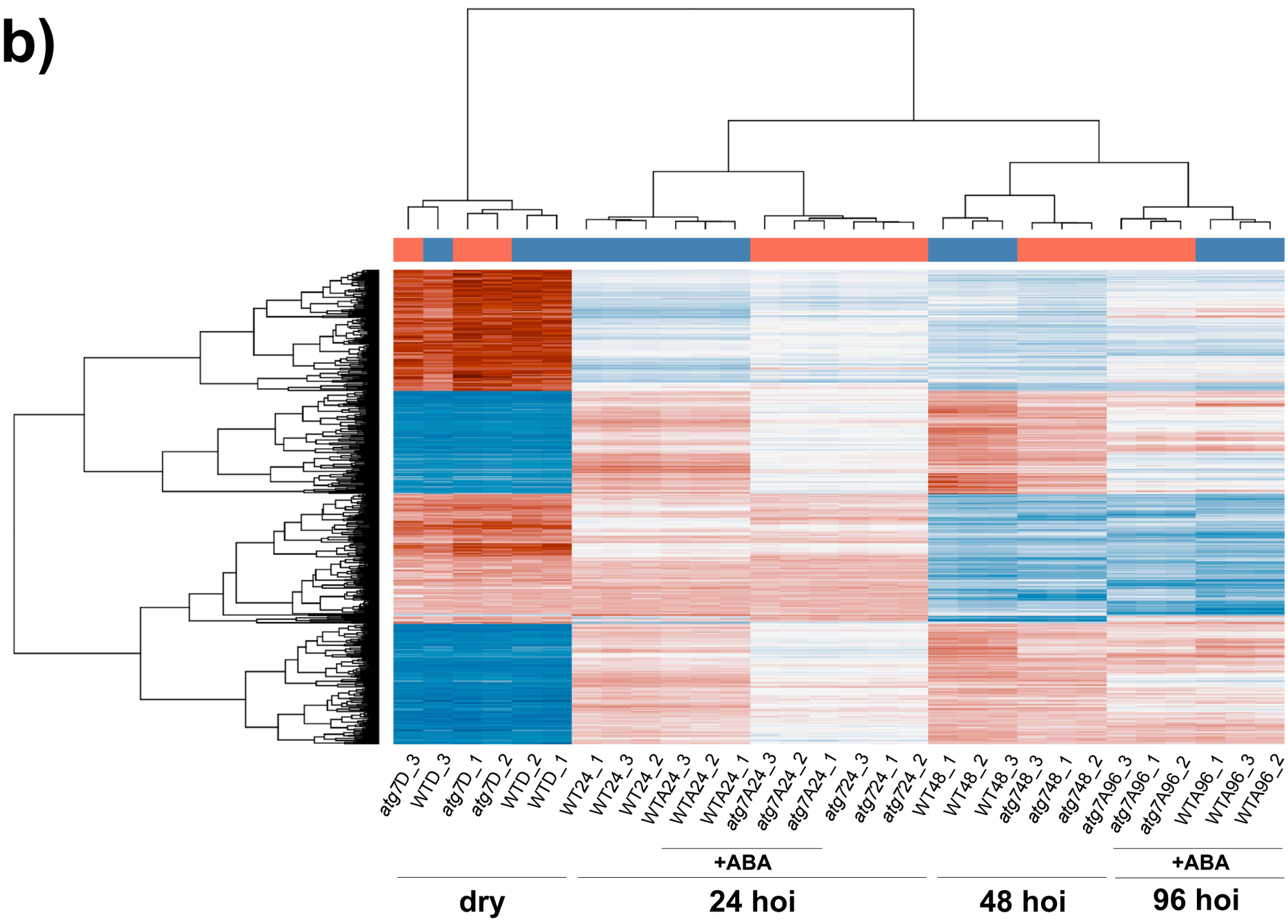

(c)

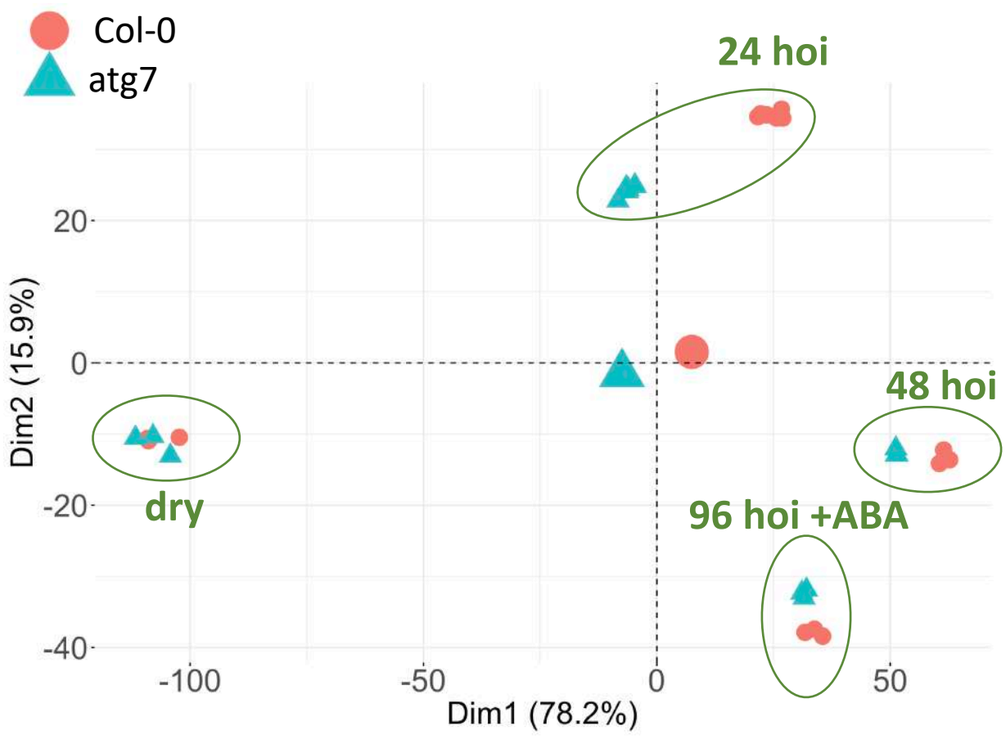

(d)

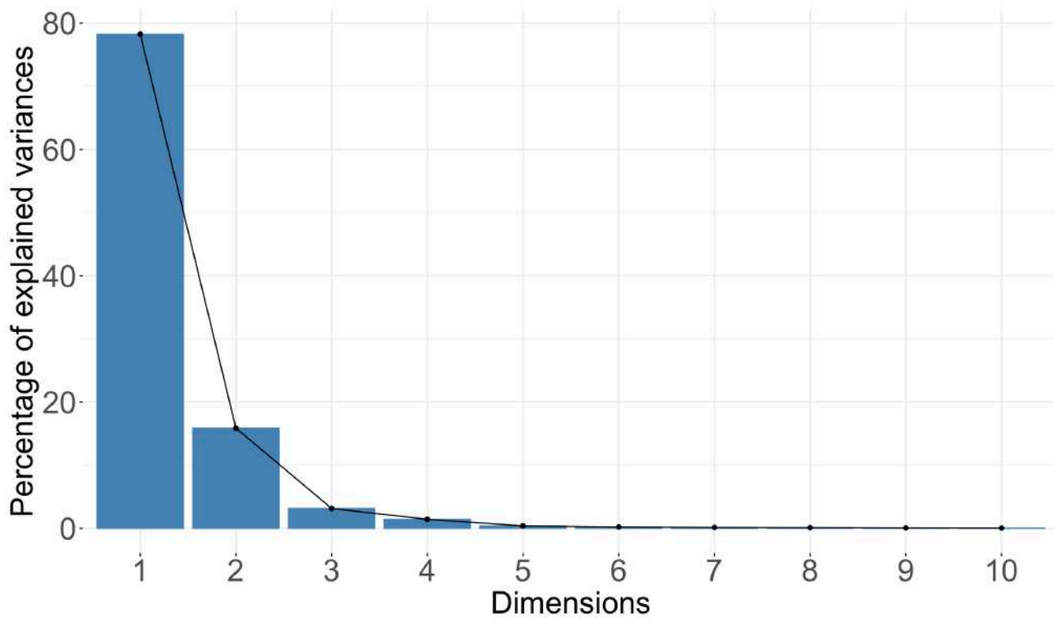

Figure S6

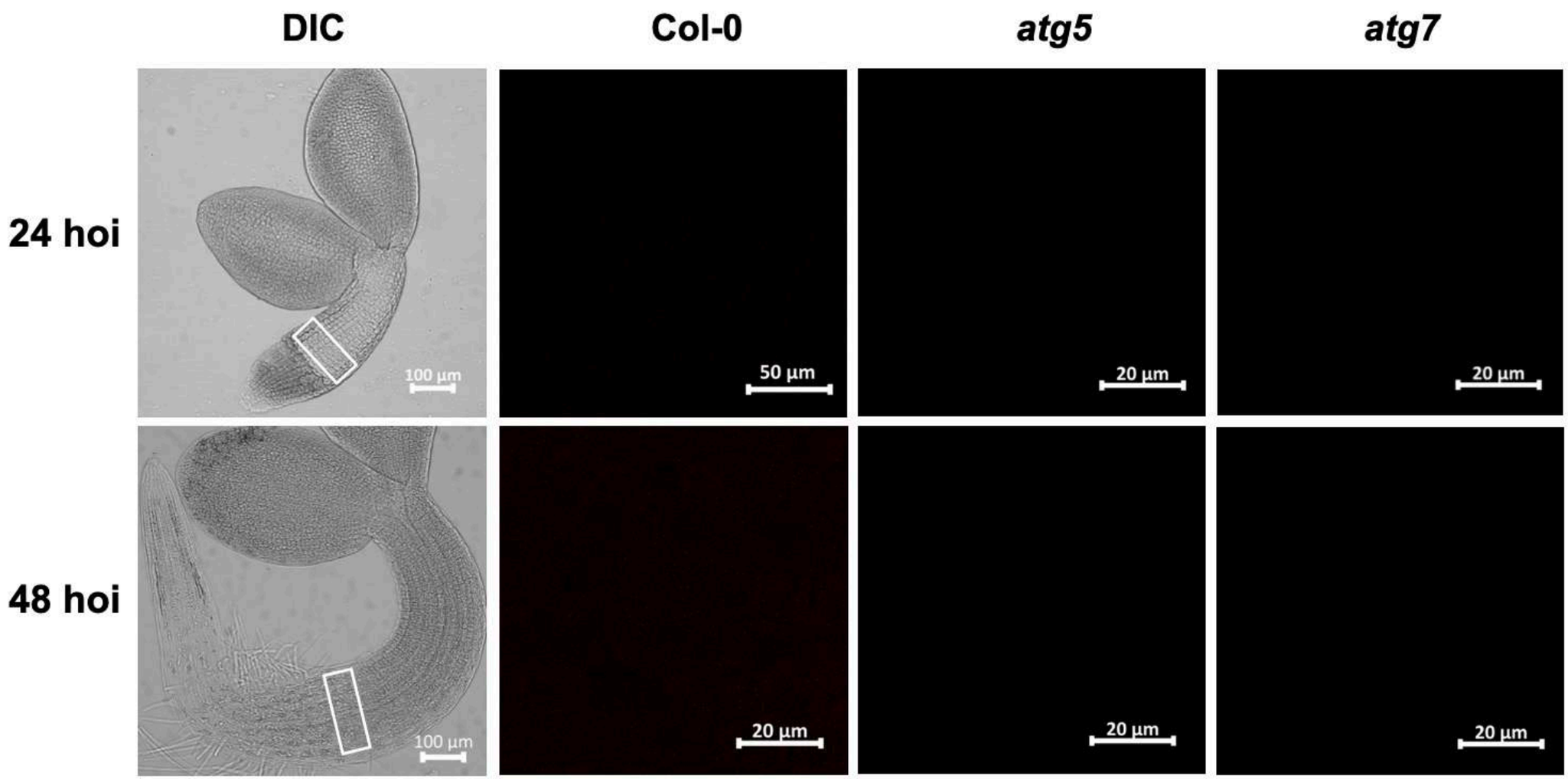
DIC
Col-0
atg5
atg7
24 hoi
48 hoi
100 µm
50 µm
20 µm
20 µm
100 µm
20 µm
20 µm
20 µm

Figure S7

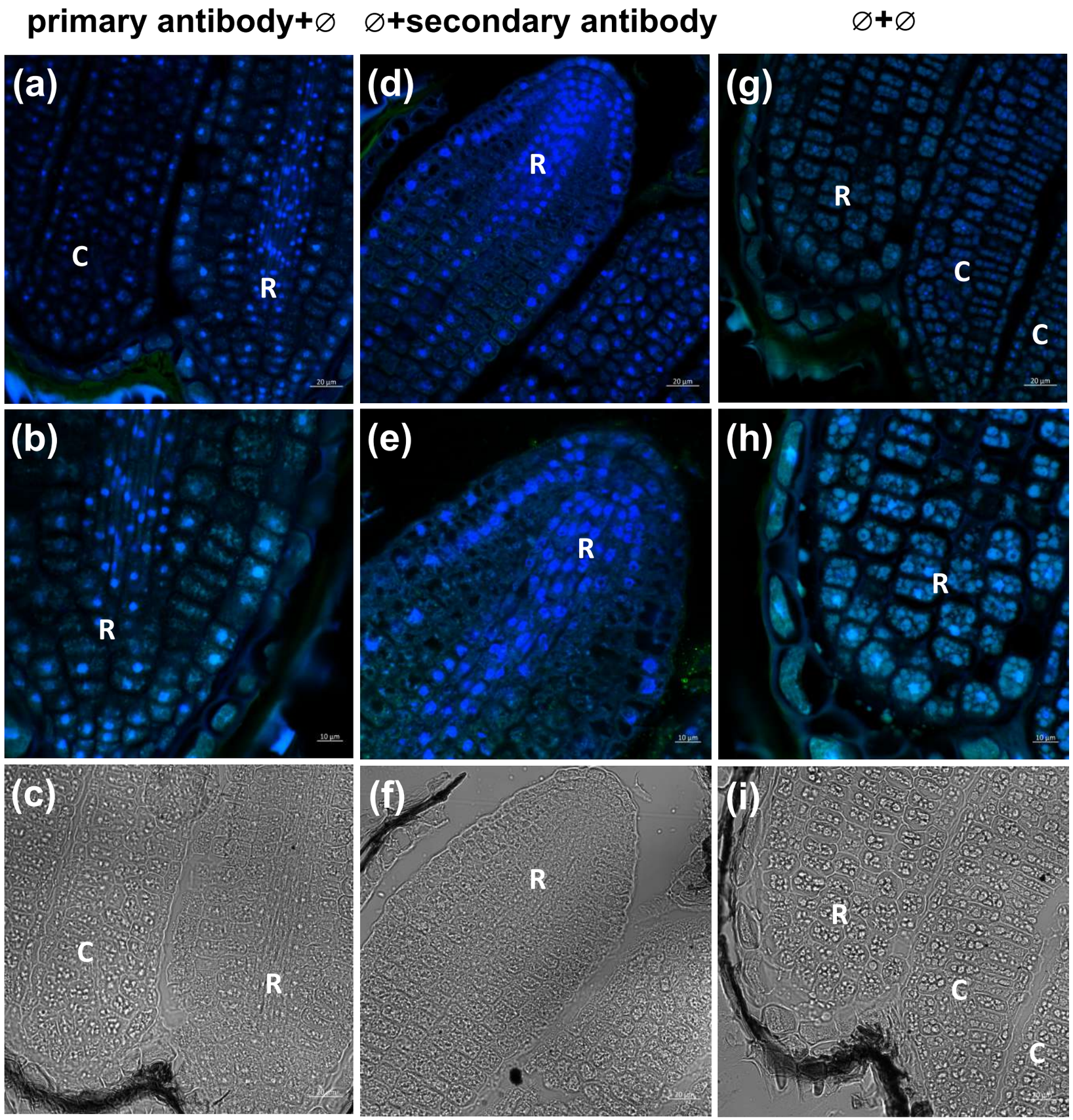
primary antibody+∅
∅+secondary antibody
∅+∅
(a)
C
R
(d)
R
(g)
R
C
C
(b)
R
(e)
R
(h)
R
(c)
C
R
(f)
R
(i)
R
C
C

Figure S8

ABI3

MKSLHVAANAGDLAEDCGILGGDADDTVLMDGIDEVGREIWLDDHGGDNNHVHGHQDDDL
IVHHDPSIFYGDLPTLPDFPCMSSSSSSSTSPAPVNAIVSSASSSSAASSSTSSAASWAI
LRSDGEDPTPNQNQYASGNCDDSSGALQSTASMEIPLDSSQGFGCGEGGGDCIDMMETFG
YMDLLDSNEFFDTSAIFSQDDDTQNPNLMDQTLERQEDQVVVPMMENNSGGDMQMMNSSL
EQDDDLAAVFLEWLKNNKETVSAEDLRKVKIKKATIESAARRLGGGKEAMKQLLKLILEW
VQTNHLQRRRTTTTTTNLSYQQSFQQDPFQNPNPNNNNLIPPSDQTCFSPSTWVPPPPQQ
QAFVSDPGFGYMPAPNYPPQPEFLPLLESPPSWPPPPQSGPMPHQQFPMPPTSQYNQFGD
PTGFNGYNMNPYQYPYVPAGQMRDQRLLRLCSSATKEARKKRMARQRRFLSHHHRHNNNN
NNNNNNQQNQTQIGETCAAVAPQLNPVATTATGGTWMYWPNVPAVPPQLPPVMETQLPTM
DRAGSASAMPRQQVVPDRRQGWKPEKNLRFLLQKVLKQSDVGNLGRIVLPKKEAETHLPE
LEARDGISLAMEDIGTSRVWNMRYRFWPNNKSRMYLLENTGDFVKTNGLQEGDFIVIYSD
VKCGKYLIRGVKVRQPSGQKPEAPPSSAATKRQNKSQRNINNNSPSANVVVASPTSQTVK

ABI5

MVTRETKLTSEREVESSMAQARHNGGGGGENHPFTSLGRQSSIYSLTLDEFQHALCENGK
NFGSMNMDEFLVSIWNAEENNNNQQQAAAAAGSHSVPANHNGFNNNNNNGGEGGVGVFSG
GSRGNEDANNKRGIANESSLPRQGSLTLPAPLCRKTVDEVWSEIHRGGGSGNGGDSNGRS
SSSNGQNNAQNGGETAARQPTFGEMTLEDFLVKAGVVREHPTNPKPNPNPNQNQNPSSVI
PAAAQQQLYGVFQGTGDPSFPGQAMGVGDPSGYAKRTGGGGYQQAPPVQAGVCYGGGVGF
GAGGQQMGMVGPLSPVSSDGLGHGQVDNIGGQYGVDMGGLRGRKRVVDGPVEKVVERRQR
RMIKNRESAARSRARKQAYTVELEAELNQLKEENAQLKHALAELERKRKQQVKTPIEFAL
LRWLQYFGQKKTTKWNCWFMVAVF

Figure S9

(a)

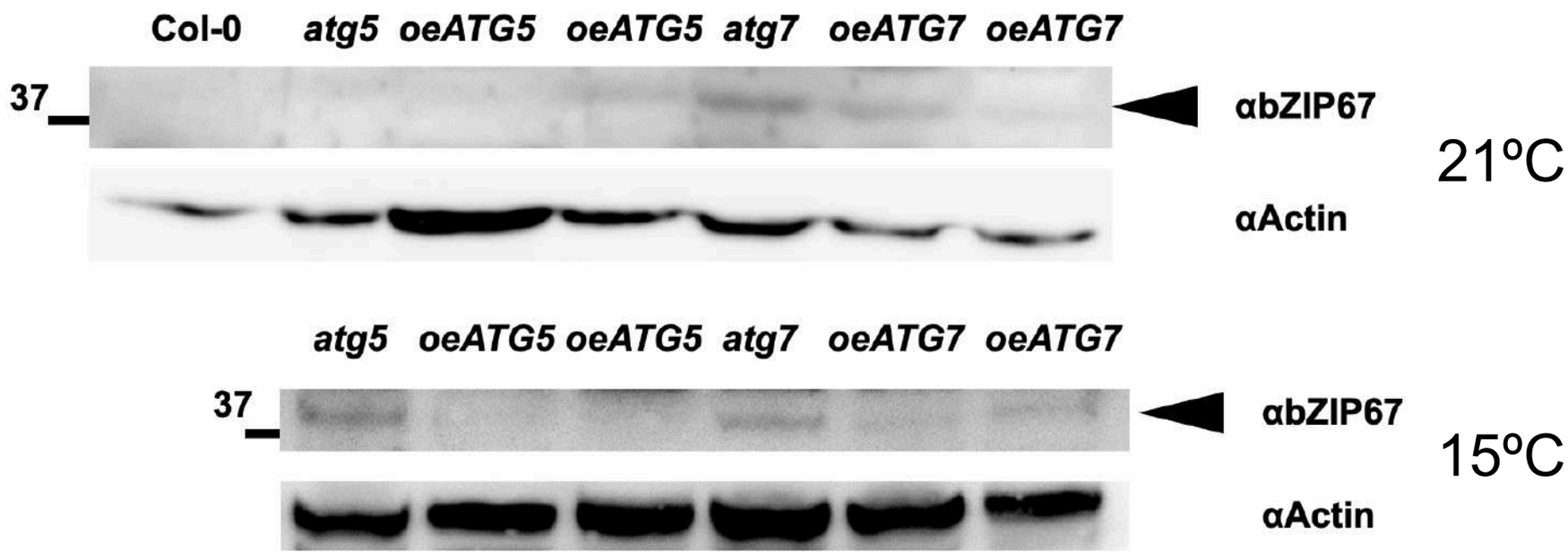

(b)

```
MSVFESETSNFHVYNNHEIQTQPQMQTFLSEEEPVGR
QNSILSLTLDEIQMKSGKSFGAMNMDEFLANLWTTVE
ENDNEGGGAHNDGEKPAVLPRQGSLSLPVPLCKKTVD
EVWLEIQNGVQQHPPSSNSGQNSAENIRRQQTLGEIT
LEDFLVKAGVVQEPLKTTMRMSSSDFGYNPEFGVGLH
CQNQNNYGDNRSVYSENRPFYSVLGESSSCMTGNGRS
NQYLTGLDAFRIKKRIIDGPPEILMERRQRRMIKNRE
SAARSRARRQAYTVELELELNNLTEENTKLKEIVEEN
EKKRRQEIISRSKQVTKEKSGDKLRKIRRMASAGW
```

(c)

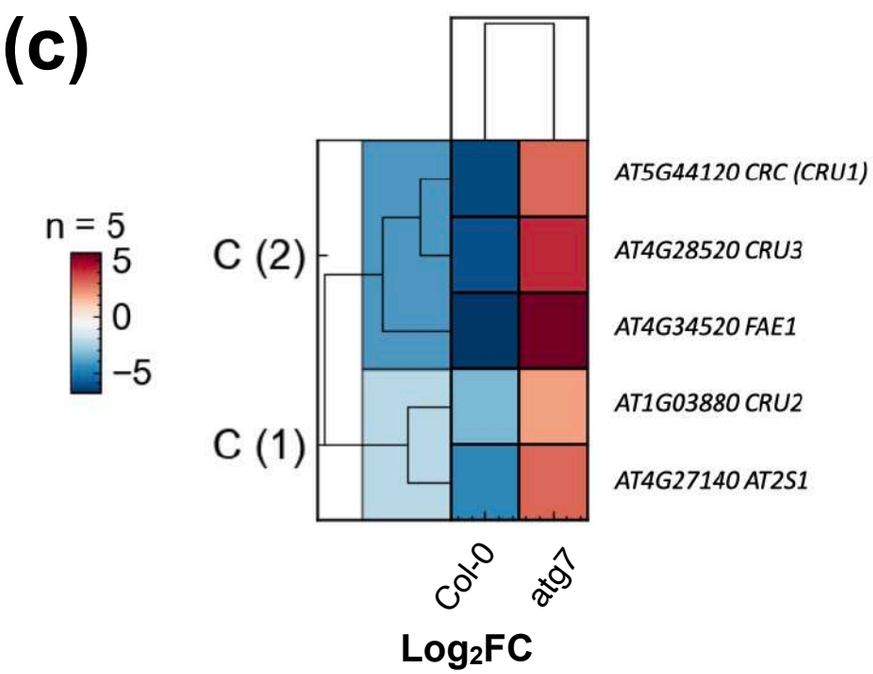

Table S1

Primers used for quantitative PCR

Gene		Primer sequence	Tm (ºC) of PCR product	Amplification product size (bp)	Amplification efficiency (%)	Regression coefficient (r^2)
ATG5	F	CTGTCCTTGTGAAAGCTCCTC	74,8	105	81	0,99
	R	CGGATTTGTAAGATGGAACG				
ATG7	F	CGGAGTATAGGGAGAGAGGAAAC	73,9	135	98	0,88
	R	TATCATCGTCTTCCCAGTCGAG				
ACT8	F	TTTCGTACACAACACTCTTCCTC	77,2	96	Graeber *et al.,* 2011	
	R	AGAACCCGTCTTCTTCCTTG				
ABI5	F	GTTTGAAGTCAAGGGCACAAC	76,9	72	92	0,99
	R	TCGGGTTCCTCATCAATGTC				

Promoter amplification primers for GUS assays

ATG5	F	GTCGACATTGATGGTTCAACA
	R	GGATCCCGCCATTCTCTTC
ATG7	F	GTCGACGCATATGCACAATCA
	R	GGATCCAGCCATGGCTGATC

Cloning primers used for yeast two hybrid

ATG8	F	GAATTCATGGGGATTGTTGTCAAGT
	R	CTCGAGTTAGCCGAAAGTTTTCTCGGT

Sequencing primers

M13	F	GTAAAACGACGGCCAGT
	R	CATGGTCATAGCTGTTTCC